

July 21, 2017

Climate of the Past Editorial Office

Dear Martin,

We would like to submit our revised manuscript entitled “Holocene dynamics in the Bering Strait inflow to the Arctic and the Beaufort Gyre circulation based on sedimentary records from the Chukchi Sea” by Yamamoto et al. We thank you, Dr. Cronin and an anonymous reviewer for helpful comments. We revised the manuscript according to your and reviewers’ comments.

Editor’s comments: Your paper has now been seen by two reviewers. Both find the paper worth publication after revision. I concur with the two reviewers as I also find that this version has been considerably improved with respect to the main critique raised by the reviewers on your earlier submitted version; that the data was over interpreted. In your point by point response to reviewer 1, it is explained how the comments will be addressed in a revision. I find that this is all in order, please infer the corrections as you have suggested you will do. The discussion on the significance of the proxy C/I and (C+K)/I, whether or not it is capable of capturing variations of the Bering Strait inflow, is crucial to the conclusions. For this reason, I would like to see some more of the reasoning you make in the interactive comment in the actual paper. I therefore suggest that you add a bit in the Discussion on this topic. I look forward to see your revised version of the paper considering the comments made by the two reviewers.

Reply: Thank you for your decision and comments. We revised our manuscript according to both reviewers’ comments. The reasoning we make in the interactive comment is added in Summary and Conclusions section in lines 733 to 741.

Reply to anonymous referee #1 on “Holocene dynamics in the Bering Strait inflow to the Arctic and the Beaufort Gyre circulation based on sedimentary records from the Chukchi Sea” by Masanobu Yamamoto et al.

We thank anonymous referee #1 for his/her helpful comments on our manuscript. Below is our reply to the main comments.

Comment: This paper deals with sediment cores from the Chukchi Sea and uses XRD mineralogy to study variability of the Beaufort Gyre and Pacific inflow into the Arctic Ocean during the Holocene. This submission is a revised version of an earlier manuscript published in Climate of the Past Discussions. One of the main comments on the original manuscript was the over-interpretation of results and linkage to Atlantic teleconnections. This component is toned down here, which has improved the manuscript. Several other reviewers' comments from the original remain, however, unaddressed so some are repeated here. This study provides a wealth of new data and new insights on the Chukchi Sea in the Holocene. I can recommend publication of this manuscript, provided the authors address the following comments and suggestions for revision.

Reply: Thank you for recognizing the significance of our paper. We revised it according to your suggestions.

Comment: Problems with C/I and (C+K)/I as proxies for Bering Strait inflow: - how solid is this proxy, if it does not show any difference (in core 5JPC, Figure 3B) between the Holocene and the last glacial when the strait was closed? - The records from the three cores show very little agreement for these proxies. Again, what does this mean for the proxy? It does not seem a convincing record of Bering inflow.

Reply: Indeed, two samples near the bottom (1600 cm) of core 5JPC have the same CK/I and C/I ratios as those of Holocene sediments. However, glacial/deglacial depositional and circulation environments were very different from the Holocene, as exemplified by abundant detrital carbonates with the Laurentide provenance. Likewise, under environments non-analogous to the Holocene, clay minerals may have had a different provenance, with chlorite possibly transported from a source other than the Bering Sea. Some intervals in the deglacial unit in 05JPC are characterized by high abundance of kaolinite and terrestrial soil organic matter (branched GDGTs), probably delivered from inland North America by deglacial discharge (Suzuki et al., AGU fall

meeting 2016). Chlorite may have also been delivered from areas affected by the Laurentide glaciation this period.

The bottom line is that glacial/deglacial records cannot be used for characterizing Holocene conditions. In comparison, the spatial distribution of clay minerals in surface sediments suggests that the Bering Strait inflow provides a major contribution of chlorite-rich sediments under modern settings. As depositional conditions in the Chukchi Sea do not appear to have changed principally in the Holocene, there is enough reason to apply the modern-type provenance pattern to understanding Holocene changes in the Bering Strait inflow.

We also recognize somewhat different patterns of C/I and CK/I among the three cores investigated. We are assuming that such a difference can be attributed to variable sediment focusing at different water depth and redistribution of the Bering Strait water between different branches after passing Bering Strait (lines 549 to 564). Further studies using more cores, e.g., from a depth transect, are required to clarify this issue.

Page 9. Lines 206-210. The top of core 01A-GC is assumed to be of modern age, because the authors write that sterols and IP25 show a decreasing trend in the top 10 cm (Stein et al 2017). This is a very poor indicator of recovery of the top sediments. Looking at the data in Stein et al 2017, the statement is not even accurate. The variability in the top 10 cm is of the same order of magnitude as deeper in the core. I suggest that this is removed (lines 206-210) and that it is acknowledged that the core top age is uncertain. There are no Pb210 dates, or a surface core to correlate with. There should be a table with radiocarbon dates and paleointensity datums (depth, age, reference). It would summarize the information spread out over pages 9-10 and shown in Figure 3. I suggest bringing back Table 1 from the original submission, adding the magnetic datums, and addressing the original reviewer comments to this version.

Reply: We agree that the core top in ARA 01-GC may not represent the modern age due to some sediment loss in the coring process. This is indicated by the absence of oxidized brown sediment at the core top, as opposed to a multi-corer collected at the same site. Nevertheless, we believe that the top of 01-GC is close to the sediment surface based on the biomarker distribution. Fig. 1 (attached below) is the concentration profile of IP25 and brassicasterol (Stein et al., 2017). We suppose that the downward decrease in

concentrations of both compounds in the top 10 cm indicates their degradation with burial. A similar extent of brassicasterol concentration decrease occurs also in some of the deeper intervals, but is unique for the upper ~200 cm, while the IP25 decrease at the top is unique for the entire record.

We provided according explanations to this part and indicate that the core-top age is uncertain (Line 249 to 258). We brought back Table 1 with the paleomagnetic datums as supplementary table 2.

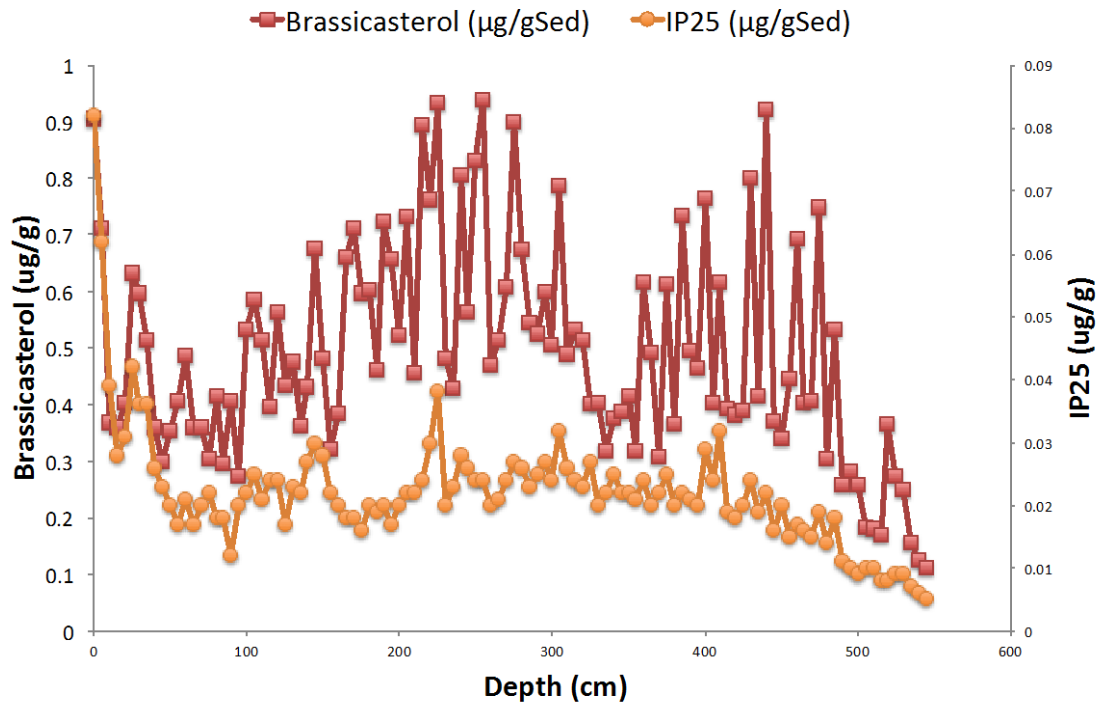


Fig. 1. Concentrations of brassicasterol and IP25 in core 01A-GC (Stein et al., 2017).

Divide section 3 in subsections: e.g. 3.1 Coring and Sampling, 3.2 Chronology, 3.3 XRD Mineralogy

Reply: We divided section 3 into subsections 3.1. Coring and Sampling, 3.2. Chronology, 3.3. XRD mineralogy, as suggested.

Figure 2 - From Panel E, one can see that there should be a data point with a CK/I ratio around 2.0 at about 63_N. This is not visible in Panel B. Check this carefully, as

there may be others? - At some sites, there are too many data points for this type of plot. An example: In Panel A, at the Mackenzie delta there are a lot of yellow dots, but they are covering up green ones as well. Either, make inserts for those areas, or make the dots smaller? - Panel E. The regression lines in CK/I and C/I vs latitude do not extend further south than 65N. Correct this or explain why.

Reply: The symbol of the sample having a CK/I of 2.0 in the Yukon River estuary is hidden by another sample in Fig. 2B. Enlarged maps for Mackenzie and Yukon River estuary areas are put in supplementary material (Supplementary Figs. 1 and 2). The regression lines show the trend for the Chukchi Sea. This suffices to show a northward decrease of the ratios north of Bering Strait. The Bering Sea sediments do not show a systematic trend, probably reflecting multiple sources of chlorite, such as the Yukon River, Aleutian Island, etc. We added according explanations in the caption of Fig. 2.

Figure 3. What do the crosses represent? Radiocarbon dates, paleointensity datums? Please specify. Add them all to a table (perhaps supplementary).

Reply: Crosses represent radiocarbon dates in 01-GC and 5JPC and paleointensity datums in 06JPC. We added this information in the caption. All datums are shown in supplementary table 2.

Figure 3. Rather than showing "D" for dolomite rich layers, please show the actual dolomite data. Also, add to the methods how dolomite was quantified (lines 250-260), and add the data to the supplementary tables.

Reply: Dolomite intensity was added in Fig. 3, and the method was added to the text (lines 346 and 347). The data are presented in supplementary tables 4 and 5.

Figure 3B. Please make it possible to distinguish between samples from the piston core vs trigger core by using different symbols.

Reply: We showed open circle symbols for 05TC samples in Fig. 3B.

Figure 4B. Same comment. Around 4000 cal yrs BP, there seem to be two data points for the same age. Is one JPC and one TC? The difference in their C/I values are large. Does this illustrate the uncertainty of the method?

Reply: Both samples were derived from core 5JPC (392 and 398 cm). The difference in the values is larger than the analytical error. We assume that this difference could be related to a high-amplitude fluctuation that was observed at the same stratigraphic level in core 01-GC. We added an according explanation (Lines 430 to 433).

Page 22 line 515. Correct “brassicasterol”.

Reply: This is corrected.

Page 23 line 538. Add citation to Jakobsson et al 2017 Climate of the Past (this same special issue).

Reply: Jakobsson et al. (2017) is cited.

Reply to referee #2 (Dr. T. M. Cronin) on “Holocene dynamics in the Bering Strait inflow to the Arctic and the Beaufort Gyre circulation based on sedimentary records from the Chukchi Sea” by Masanobu Yamamoto et al.

We thank Dr. Cronin for his helpful comments on our manuscript. Below is our reply to the main comments.

Comment: This is a good paper on Holocene variability in a key part of the Arctic based on 3 sediment cores with decent chronology. The attached PDF has a number of comments inserted, including many minor problems with English.

Reply: Thank you for recognizing the significance of our paper. We revised it according to your suggestions. Minor English problems were corrected as commented.

But the most important problem with the paper is the confusing discussions in several places about the causes of variability in the mineralogical proxies used [if we accept the authors' ideas on what these proxies signify in terms of sea ice and ocean circulation]. Giving the benefit of the doubt on proxies, the paper should simplify mechanisms to explain patterns: long term insolation change during the Holocene, millennial-centennial TSI solar forcing, sea-level wind etc forcing Bering Strait inflow, the Arctic Oscillation affecting the Beaufort Gyre and Transpolar drift. Can these few mineralogical indices really distinguish among all these factors? Instead, can the authors highlight those patterns that are most important, like the shift in circulation near 1000 years ago. Or the early Holocene thermal warming. Or just the sea ice history? In the final revision, please make it easier for readers to see the main take-home messages and which hypotheses are supported.

Reply: To simplify the explanation of the identified paleoceanographic changes, we have added the following table (Table 1) summarizing the patterns of the paleo-BG circulation and BSI, along with their possible forcings.

Table 1. Summary of Holocene variability in the BG and BSI in northern Chukchi Sea

Current system	Holocene trends	Multi-centennial to millennial cyclicality
Beaufort Gyre (BG) circulation	Gradual weakening in response to decreasing summer insolation	~0.36, 0.5, 1, and 2-kyr cycles paced by changes in solar activity
Bering Strait inflow (BSI)	Geographically variable. Mid-Holocene strengthening evident at the 01A-GC site, presumably due to weaker Aleutian Low	Geographically variable. ~0.36, 0.5, 1, and 2-kyr cycles paced by changes in solar activity are identifiable in 01A-GC

Line 84: Can you quantify the BSI in terms of its contribution in heat flow, relative to other ocean, atmospheric sources? Or just volume in Sverdrups compared to the other exchange routes into the Arctic? I guess some is covered below.

Reply: We have added the following clarification in the introduction: “Mooring data suggest that an increase in the BSI volume by ~50% from 2001 (~0.7 Sv) to 2011 (~1.1 Sv) has driven an according increase in the heat flux from $\sim 3 \times 10^{20}$ J to $\sim 5 \times 10^{20}$ J (Woodgate et al., 2012).” (Lines 98 to 101)

Line 222: Is there an alternative possible age model? The age for the base of the core is really important.

Reply: At this point, no chronostratigraphic constraint is available for the lower part of the core, below the occurrence of material suitable for radiocarbon dating. Glaciomarine sediments were clearly deposited in sedimentological conditions different from those of the marine Holocene unit, which precludes the extrapolation of sedimentation rates derived from the ^{14}C ages to the core bottom.

Line 407: This is a huge conclusion, perhaps requiring more rigorous statistics and mechanistic explanation.

Reply: We do not see anything unexpected or sensational in this conclusion. It is

consistent with data from other Holocene studies (Hu et al., 2008; Anderson et al., 2005; Fisher et al., 2004; Sagawa et al., 2014), including the Chukchi shelf (Stein et al., 2017). We have revised the sentence to “This pattern suggests that millennial-scale variability in the BG was principally forced by changes in solar irradiance as the most likely forcing. Proxy records consistent with solar forcing were reported from a number of paleoclimatic archives, such as Chinese stalagmites (Hu et al., 2008), Yukon lake sediments (Anderson et al., 2005) and ice cores (Fisher et al., 2008), as well as marine sediments in the northwestern Pacific (Sagawa et al., 2014) and the Chukchi Sea (Stein et al., 2017).” (Lines 509 to 515)

Line 485: check throughout the paper sea-ice versus sea ice [no hyphen] when used as an adjective.

Reply: Corrected.

Line 558: what is the island rule?

Reply: The island rule is a concept used for modeling the direction and flow volume of an ocean current along the coast of an island or continent under a certain wind stress field (Godfrey, 1989). We, however, realize that the mention of the Island Rule is not necessary in this paper, so we have removed the phrase “based on the island rule (Godfrey, 1989).”

Line 611: Can you make conclusions in bullet form? There is confusion about insolation, TSI-Solar forcing versus other processes in the BSI inflow. Also the AO mode of variability seems prominent, but no discussion of Pacific multidecadal PDO var.

Reply: This section has been expanded to provide more explanation to the main conclusions, and a brief summary has been added in Table 1. We note that our records show multi-centennial and millennial-scale variability in the BG circulation and the BSI, which both seem to respond to changes in solar activity. To what extent the AO and PDO are involved in the BG and BSI dynamics is less clear and requires further investigation (see discussion in sections 5.1 and 5.6).

1 **Holocene dynamics in the Bering Strait inflow to the Arctic and the Beaufort Gyre**
2 **circulation based on sedimentary records from the Chukchi Sea**

3

4 Masanobu Yamamoto^{1-3*}, Seung-Il Nam⁴, Leonid Polyak⁵, Daisuke Kobayashi³, Kenta
5 Suzuki³, Tomohisa Irino^{1,3}, Koji Shimada⁶

6

7 *¹Faculty of Environmental Earth Science, Hokkaido University, Kita-10, Nishi-5,
8 Kita-ku, Sapporo 060-0810 Japan*

9 *²Global Institution for Collaborative Research and Education, Hokkaido University,
10 Kita-10, Nishi-5, Kita-ku, Sapporo 060-0810 Japan*

11 *³Graduate School of Environmental Science, Hokkaido University, Kita-10, Nishi-5,
12 Kita-ku, Sapporo 060-0810 Japan*

13 *⁴Korea Polar Research Institute, 26 Songdomirae-ro, Yeonsu-gu, Incheon 21990,
14 Republic of Korea*

15 *⁵Byrd Polar and Climate Research Center, The Ohio State University, Columbus, OH
16 43210USA*

17 *⁶Tokyo University of Marine Science and Technology, 4-5-7, Konan, Minato-ku, Tokyo
18 108-8477, Japan.*

19 **Corresponding author. Tel: +81-11-706-2379, Fax: +81-11-706-4867, E-mail address:
20 myama@ees.hokudai.ac.jp (M. Yamamoto)*

21

22 **ABSTRACT**

23 The Beaufort Gyre (BG) and the Bering Strait inflow (BSI) are important elements of
24 the Arctic Ocean circulation system and major controls on the distribution of Arctic sea

25 ice. We report records of the quartz/feldspar and chlorite/illite ratios in three sediment
26 cores from the northern Chukchi Sea providing insights into the long-term dynamics of
27 the BG circulation and the BSI during the Holocene. The quartz/feldspar ratio, a proxy
28 of the BG strength, gradually decreased during the Holocene, suggesting a long-term
29 decline in the BG strength, consistent with orbitally-controlled decrease in summer
30 insolation. We suppose that the BG rotation weakened as a result of increasing stability
31 of sea-ice cover at the margins of the Canada Basin, driven by decreasing insolation.
32 Millennial to multi-centennial variability in the quartz/feldspar ratio (the BG
33 circulation) is consistent with fluctuations in solar irradiance, suggesting that solar
34 activity affected the BG strength on these timescales. The BSI approximated by the
35 chlorite/illite record, despite a considerable geographic variability, consistently shows
36 intensified flow from the Bering Sea to the Arctic during the middle Holocene, which is
37 attributed primarily to the effect of higher atmospheric pressure over the an overall
38 weaker Aleutian Low pressure center Basin. The ~~middle Holocene~~ intensification of
39 ~~the~~ BSI was associated with decrease in sea ice concentrations and increase in
40 marine production, as indicated by biomarker concentrations, suggesting a major
41 influence of the BSI on sea ice distribution and biological production conditions
42 in the Chukchi Sea. Multi-century to millennial fluctuations, presumably controlled by
43 solar activity, were also identified in a proxy-based BSI record characterized with the
44 highest age resolution.

46 1. Introduction

47 The Arctic currently faces rapid climate change caused by global warming (e.g.,
48 Screen and Simmonds, 2010; Harada, 2016). Changes in the current system of the

49 Arctic Ocean regulate the state of Arctic sea ice and are involved in global processes via
50 ice albedo feedback and the delivery of freshwater to the North Atlantic Ocean (Miller
51 et al., 2010; Screen and Simmonds, 2010). The most significant consequence of this
52 climate change during recent decades is the retreat of summer sea ice in the Pacific
53 sector of the Arctic (e.g., Shimada et al., 2006; Harada et al., 2016, and references
54 therein). Inflow of warm Pacific water through the Bering Strait (hereafter Bering Strait
55 Inflow [BSI]) is suggested to have caused catastrophic changes in ~~sea-ice~~[sea-ice](#)
56 stability in the western Arctic Ocean (Shimada et al., 2006). Comprehending these
57 changes requires investigation of a longer-term history of circulation in the western
58 Arctic and its relationship to atmospheric forcings. Within this context, the Chukchi Sea
59 is a key region to understand the western Arctic current system as it is located at the
60 crossroads of the BSI and the Beaufort Gyre (BG) circulation in the western Arctic
61 Ocean (Fig. 1) (e.g., Winsor and Chapman, 2004; Weingartner et al., 2005).

62 In this paper we apply mineralogical proxies of the BG and BSI to sediment cores
63 with a century-scale resolution from the northern margin of the Chukchi shelf. The
64 generated record provides new understanding of changes in the BG circulation and BSI
65 strength during most of the Holocene (last ~9 ka). We discuss the possible causes and
66 forcings of the BG and BSI variability, as well as its relationship to sea-ice history and
67 biological production in the western Arctic.

68

69 **2. Background information**

70 *2.1. Oceanographic settings*

71 The wind-driven surface current system of the Arctic Ocean consists of the BG and
72 the Transpolar Drift (TPD) (Proshutinsky and Johnson, 1997; Rigor et al., 2002). This

73 circulation is controlled by the atmospheric system known as the Arctic Oscillation
74 (AO) (Rigor et al., 2002). When the AO is in the positive phase, the BG shrinks back
75 into the Beaufort Sea, the TPD expands to the western Arctic Ocean, and the sea-ice
76 transport from the eastern Arctic to the Atlantic Ocean is intensified. When the AO is in
77 negative phase, the BG expands, the TPD is limited to the eastern Arctic, and sea ice is
78 exported efficiently from the Canada Basin to the eastern Arctic. Thus, sea-ice
79 distribution is closely related to the current system.

80 A dramatic strengthening of the BG circulation occurred during the last two decades
81 (Shimada et al., 2006; Giles et al., 2012). This change was attributed to a recent
82 reduction in sea-ice cover along the margin of the Canada Basin, which caused a more
83 efficient transfer of the wind momentum to the ice and underlying waters in the BG
84 (Shimada et al., 2006). The delayed development of sea ice in winter enhanced the
85 western branch of the Pacific Summer Water across the Chukchi Sea. This anomalous
86 heat flux into the western part of the Canada Basin retarded sea-ice formation during
87 winter, thus, further accelerating overall sea-ice reduction.

88 The BSI, an important carrier of heat and freshwater to the Arctic, transports the
89 Pacific water to and across the Chukchi Sea, interacts with the BG circulation at the
90 Chukchi shelf margin (e.g., Shimada et al., 2006). Mooring data suggest that an increase
91 in the BSI increases volume by ~5450% from 2001 (~0.7 Sv) to 2011 (~1.1 Sv); has
92 drivening an according increase in the heat flux increases from $\sim 3 \times 10^{20}$ J in 2001 to ~ 5
93 $\times 10^{20}$ J in 2011 (Woodgate et al., 2012). After passing the Bering Strait the BSI flows
94 in three major branches. One branch, the Alaskan Coastal Current (ACC), runs
95 northeastward along the Alaskan coast as a buoyancy-driven boundary current (Red
96 arrow in Fig. 1; Shimada et al., 2001; Pickart, 2004; Weingartner et al., 2005). The

97 second, central branch follows a seafloor depression between Herald and Hanna Shoals,
98 then turns eastward and merges with the ACC (Yellow arrow in Fig. 1; Winsor and
99 Chapman, 2004; Weingartner et al., 2005). The third branch flows northwestward,
100 especially when easterly winds prevent the ACC (Winsor and Chapman, 2004). This
101 branch may then turn eastward along the shelf break (Blue arrow in Fig. 1; Pickart et al.,
102 2010).

103 The BSI is driven by a northward dip in sea level between the North Pacific and the
104 Arctic Ocean (Shtokman, 1957; Coachman and Aagaard, 1966). There has been a
105 long-standing debate, whether this dipping is primarily controlled by steric difference
106 (Stigebrandt, 1984) or from wind-driven circulations (Gudkovitch, 1962). Stigebrandt
107 (1984) assumed that the salinity difference between the Pacific and Atlantic Oceans
108 causes the steric height difference between the Bering Sea and the Arctic Ocean.
109 Aagaard et al. (2006) argued that the local salinity in the northern Bering Sea controlled
110 the BSI, although wind can considerably modify the BSI on a seasonal timescale. De
111 Boer and Nof (2004) proposed a model that the mean sea level difference along the
112 strait is set up by the global winds, particularly the strong Subantarctic Westerlies.

113 Recently, a conceptual model of the BSI controls has been developed based on a
114 decade of oceanographic observations (Danielson et al., 2014). According to this model,
115 storms centered over the Bering Sea excite continental shelf waves on the eastern
116 Bering shelf that intensify the BSI on synoptic time scales, but the integrated effect of
117 these storms tends to decrease the BSI on annual to decadal time scales. At the same
118 time, an eastward shift and overall strengthening of the Aleutian Low pressure center
119 during the period between 2000–2005 and 2005–2011 increased the sea level pressure
120 in the Aleutian Basin south of the Bering Strait by 5 hPa, in contrast to overall

121 decreased pressure of the Aleutian Low system, thus decreasing the water column
122 density through isopycnal uplift by weaker Ekman suction. This change thereby raised
123 the dynamic sea surface height by 4.2 m along the Bering Strait pressure gradient,
124 resulting in the BSI increase by 4.5 cm/s, or 0.2 Sv (calculated based on the
125 cross-section area of $4.25 \times 10^6 \text{ m}^2$). This increase constitutes about one quarter of the
126 average long-term BSI volume of $\sim 0.8 \text{ Sv}$ (Roach et al., 1995). Such a large
127 contribution clearly identifies changes in the Aleutian Low strength and position as a
128 key factor regulating the BSI on inter-annual time scales.

129 | The BSI also transports nutrients from the Pacific to the Arctic. A rough estimation
130 suggests that the BSI waters significantly contribute to marine production in the Arctic
131 (Yamamoto-Kawai et al., 2006). High marine production in the Chukchi Sea of up to
132 $400 \text{ gC m}^{-2} \text{ y}^{-1}$ in part is thought to reflect the high nutrient fluxes by the BSI (Walsh
133 and Dieterle, 1994; Sakshaug, 2004). A recent enhancement of biological productivity
134 and the biological pump in the Beaufort and Chukchi Seas has been associated with the
135 retreat of sea ice (summarized by Harada et al., 2016). This phenomenon is attributed to
136 an increase of irradiance in the water column (Frey et al., 2011; Lee and Whitley,
137 2005), wind-induced mixing that replenishes sea surface nutrients (Carmack et al.,
138 2006), and their combination (Nishino et al., 2009). However, the nutrient flux into the
139 Arctic Ocean was not evaluated in this context. The investigation of BSI intensity and
140 marine production during the Holocene will be useful to understand on-going changes
141 in marine production in the Arctic Ocean.

142

143 ***2.2. Mineral distribution in the Chukchi Sea sediments***

144 Spatial variation in mineral composition of surficial sediments along the western
145 Arctic margin has been investigated in a number of studies using different
146 methodological approaches but showing an overall consistent picture (e.g., Naidu et al.,
147 1982; Naidu and Mowatt, 1983; Wahsner et al., 1999; Kalinenko, 2001; Viscosi-Shirley
148 et al., 2003; Darby et al., 2011; Kobayashi et al., 2016). A recent study of mineral
149 distribution in sediments from the Chukchi Sea and adjacent areas of the Arctic Ocean
150 and the Bering Sea suggests that the quartz/feldspar (Q/F) ratio is higher on the North
151 American than on the Siberian side of the western Arctic (Fig. 2; Kobayashi et al.,
152 2016). These results are consistent with earlier studies including mineral determinations
153 of shelf sediments and adjacent coasts (Vogt, 1997; Stein, 2008; ~~Darby et al., 2011~~). ~~In~~
154 ~~particular, data of~~ Darby et al. (2011), ~~although quantified by a different method, also~~
155 show a trend of decreasing Q/F ratio [in dirty sea ice](#) from North American margin to the
156 Chukchi Sea and further to the East Siberian Sea. This zonal gradient of the Q/F ratio
157 suggests that quartz-rich but feldspar-poor sediments are derived from the North
158 American margin by the BG circulation, whereas feldspar-rich sediments are delivered
159 to the Chukchi Sea from the Siberian margin by currents along the East Siberian slope
160 (Kobayashi et al., 2016). Thus, this ratio can be used as a provenance index for the BG
161 circulation reflecting changes in its intensity in sediment-core records (Kobayashi et al.,
162 2016).

163 Kaolinite is generally [a minor component of clays](#) in the western Arctic but relatively
164 abundant in the Northwind Ridge and Mackenzie Delta areas where the BG circulation
165 exerts an influence (Naidu and Mowatt, 1983; Kobayashi et al., 2016). Kaolinite in the
166 Northwind Ridge originated from ancient rocks exposed on the North Slope and was
167 delivered by water or sea ice via the Beaufort Gyre circulation (Kobayashi et al., 2016).

168 Kobayashi et al. (2016) also indicate that both the (chlorite + kaolinite)/illite and
169 chlorite/illite ratios (CK/I and C/I ratios, respectively) are higher in the Bering Sea and
170 decrease northward throughout the Chukchi Sea, reflecting the diminishing strength of
171 the BSI (Fig. 2). These results are consistent with earlier studies showing that illite is a
172 common clay mineral in Arctic sediments (Kalinenko, 2001; Darby et al., 2011),
173 whereas, chlorite is more abundant in the Bering Sea and the Chukchi shelf areas
174 influenced by the BSI (Naidu and Mowatt, 1983; Kalinenko, 2001; Nwaodua et al.,
175 2014; Kobayashi et al., 2016). Chlorite occurs abundantly near the Bering Sea coasts of
176 Alaska, Canada, and the Aleutian Islands (Griffin and Goldberg, 1963). The
177 chlorite/illite ratio is higher in the bed load of rivers and deltaic sediments from
178 southwestern Alaska than from northern Alaska and East Siberia, reflecting differences
179 in the geology of the drainage basins (Naidu and Mowatt, 1983). Because chlorite
180 grains are more mobile than illite grains under conditions of intense hydrodynamic
181 activity, chlorite grains are transported a long distance from the northern Bering Sea to
182 the Chukchi Sea via the Bering Strait (Kalinenko, 2001). In the surface sediments of the
183 Chukchi Sea, the CK/I ratio shows a good correlation with the C/I ratio, indicating that
184 both ratios can be used as a provenance index for the BSI (Kobayashi et al., 2016).

185 Ortiz et al. (2009) constructed the first chlorite-based Holocene record of the BSI by
186 quantifying the total chlorite plus muscovite abundance based on diffuse spectral
187 reflectance of sediments from a northeastern Chukchi Sea core. The record shows a
188 prominent intensification of the BSI in the middle Holocene. However, a record from
189 just one site is clearly insufficient to characterize sedimentation and circulation history
190 in such a complex area. More records of mineral proxy distribution covering various

191 oceanographic and depositional environments are needed to further our understanding
192 of the evolution of the BSI.

193 The Holocene dynamics of the BG circulation is also poorly understood. A study of
194 sediment core from the northeastern Chukchi slope identified centennial- to
195 millennial-scale variability in the occurrence of Siberian iron oxide grains presumably
196 delivered via the BG (Darby et al., 2012). However, transport of these grains depends
197 not only on the BG, but also on circulation and ice conditions in the Eurasian basin,
198 which complicates the interpretation and necessitates further proxy studies of the BG
199 history.

200

201 **3. Samples and methods**

202 [3.1. Coring and sampling](#)

203 This study uses three sediment cores from the northern and northeastern margins of
204 the Chukchi Sea: ARA02B 01A-GC (gravity core; 563 cm long; 73°37.89'N,
205 166°30.98'W), HLY0501-05JPC/TC (jumbo piston core/trigger; 1648 cm long,
206 72°41.68'N, 157°31.20'W) and HLY0501-06JPC (1554 cm long; 72°30.71'N,
207 157°02.08'W) collected from 111 m, 462 m and 673 water depth, respectively (Fig. 1).
208 The sediments in 01A-GC and in the Holocene part of 05JPC/TC (0–1300 cm) and
209 06JPC (0–935 cm) consist predominantly of homogeneous clayey silt (fine-grained
210 unit). This unit of cores 05JPC and 06JPC is underlain by a more complex
211 lithostratigraphy with laminations and coarse ice rafted debris indicative of
212 glaciomarine environments affected by glacial/deglacial processes (“glaciomarine unit”;
213 McKay et al., 2008; Lisé-Pronovost et al., 2009; Polyak et al., 2009).

214 In total 110 samples were collected for mineralogical analysis from core 01A-GC at
215 intervals averaging 5 cm, (equivalent to approximately 80–90 years (see chronology
216 description below), down to a depth of 545 cm (ca. 9.3 ka). In core 05JPC/TC, 44
217 samples were collected from fine-grained unit at intervals averaging 30 cm (equivalent
218 to approximately 210–220 years) down to a depth of 1286 cm (ca. 9.3 ka), and 7
219 samples were collected from the underlying glaciomarine sediments. In core 06JPC, 79
220 samples were collected from fine-grained unit at intervals of 10 cm (equivalent to
221 approximately 90 years) down to a depth of 937 cm (ca. 8.0 ka), and 46 samples were
222 collected from the underlying glaciomarine unit.

223 We also analyzed 16 surface sediment samples (0–1 cm) from the eastern Beaufort
224 Sea near the Mackenzie River delta and 3 surface sediment samples (0–1 cm) from the
225 western Beaufort Sea (Fig. 2) to fill the gaps in the dataset of Kobayashi et al. (2016)
226 (Fig. 2). These samples were obtained during the RV Araon cruises in 2013 and 2014
227 (ARA04C and ARA05C, respectively; supplementary table 1).

228

229 3.2. Chronology

230 Age for core 01A-GC was constrained by seven accelerator mass spectrometry
231 (AMS) ^{14}C ages of mollusc shells from core 01A-GC (Supplementary Table 2; Stein et
232 al., 2017). The core top in ARA 01-GC may not represent the modern age due to some
233 sediment loss in the coring process. This is indicated by the absence of oxidized brown
234 sediment at the core top, as opposed to a multi-corer collected at the same site.
235 Nevertheless, we believe that the top of 01-GC is close to the sediment surface based on
236 the biomarker distribution. IP_{25} and brassicasterols show a downward decreasing trend
237 in their concentrations in the top 10 cm (Stein et al., 2017). We suppose that this

238 [indicates their degradation with burial. A similar extent of brassicasterol concentration](#)
239 [decrease occurs also in some of the deeper intervals, but is unique for the upper ~200](#)
240 [cm, while the IP25 decrease at the top is unique for the entire record. ~~Because of this~~](#)
241 [reason](#)Therefore, ~~t~~The core_top of 01A-GC was assumed to ~~be represent~~ sediment
242 surface ~~in the age-depth model because labile organic compounds such as IP₂₅ and~~
243 ~~sterols show a downcore decreasing trend in their concentrations in the top 10 cm (Stein~~
244 ~~et al., 2017), which is commonly seen in ocean surface sediments, suggesting that the~~
245 ~~lost of surface sediments was minimal during coring.~~ ¹⁴C ages were converted to
246 calendar ages using the CALIB7.0 program and marine13 dataset (Reimer et al., 2013).
247 Local reservoir correction (ΔR) [for 01A-GC sited in surface waters](#) was assumed 500
248 years ~~for 01A-GC~~ (McNeely et al., 2006; Darby et al., 2012). [The age model was](#)
249 [constructed by linear interpolation between the ¹⁴C datings \(3.1–8.6 ka\). Ages below the](#)
250 [dated range were extrapolated to the bottom of core \(9.3 ka\).](#)
251 In core 05JPC/TC, age was constrained by six AMS ¹⁴C ages of mollusc shells from
252 core 05JPC ([Supplementary Table 2](#); Barletta et al., 2008; Darby et al., 2009). Local
253 reservoir correction (ΔR) was assumed [to be 0 years as the core site is washed by](#)
254 [Atlantic intermediate water for 05JPC](#) (~~McNeely et al., 2006~~; Darby et al., 2012).
255 Concurrent age constraints for 05JPC were provided by ²¹⁰Pb determinations in the
256 upper part (05TC) and paleomagnetic analysis (Barletta et al., 2008; McKay et al.,
257 2008; ~~Darby et al., 2012~~). The age model ~~of for~~ core 05JPC/TC was constructed by
258 linear interpolation between the ¹⁴C datings (2.4–7.7 ka) as well as the assumed modern
259 age of the 05TC top, with the assumption that the offset of JPC to TC is 75 cm ([Polyak](#)
260 [et al., 2016](#)~~Darby et al., 2009~~). Ages below the dated range were extrapolated to the
261 bottom of homogenous fine-grained unit at 1300 cm (9.4 ka).

262 In core 06JPC, age was tentatively constrained by ten paleointensity datums based on
263 ~~the ¹⁴C ages of nearby cores~~[regional paleomagnetic chronology](#) and a ¹⁴C age of benthic
264 foraminifera (8.16 ka at 918 cm) ([Supplementary Table 2](#); Lisé-Pronovost et al., 2009),
265 with the assumption that the offset of JPC to TC is 147 cm (Ortiz et al., 2009). The age
266 model ~~of~~[for](#) core 06JPC was constructed by linear interpolation between the
267 paleointensity datums (2.0–7.9 ka).

~~In total 110 samples were collected for mineralogical analysis from core 01A-GC at
268 intervals averaging 5 cm (equivalent to approximately 80–90 years) down to a depth of
269 545 cm (ca. 9.3 ka). In core 05JPC/TC, 44 samples were collected from fine grained
270 unit at intervals averaging 30 cm (equivalent to approximately 210–220 years) down to
271 a depth of 1286 cm (ca. 9.3 ka), and 7 samples were collected from the underlying
272 glaciomarine sediments. In core 06JPC, 79 samples were collected from fine grained
273 unit at intervals of 10 cm (equivalent to approximately 90 years) down to a depth of 937
274 cm (ca. 8.0 ka), and 46 samples were collected from the underlying glaciomarine unit.~~

276 277 [3.3. XRD mineralogy](#)

~~We also analyzed 16 surface sediment samples (0–1 cm) from the eastern Beaufort Sea
278 near Mackenzie delta and 3 surface sediment samples (0–1 cm) from the western
279 Beaufort Sea (Fig. 2) to fill the gaps in the dataset of Kobayashi et al. (2016). These
280 were obtained during the RV Araon cruises in 2013 and 2014 (ARA04C and ARA05C,
281 respectively; supplementary table 1).~~

283 Mineral composition was analyzed on MX-Labo X-ray diffractometer (XRD)
284 equipped with a CuK α tube and monochromator. The ~~used~~ tube voltage and current
285 were 40 kV and 20 mA, respectively. Scanning speed was 4°2 θ /min and the data

286 sampling step was $0.02^{\circ}2\theta$. Each powdered sample was mounted on a glass holder with
287 a random orientation and X-rayed from 2 to $40^{\circ}2\theta$. An additional precise scan with a
288 scanning speed of $0.2^{\circ}2\theta/\text{min}$ and sampling step of $0.01^{\circ}2\theta$ from 24 to $27^{\circ}2\theta$ was
289 conducted to distinguish chlorite from kaolinite by evaluation of the peaks around
290 $25.1^{\circ}2\theta$ (Elvelhøi and Rønningsland, 1978). In this study, the background-corrected
291 diagnostic peak intensity was used for evaluating the abundance of each mineral. The
292 relative XRD intensities of quartz at $26.6^{\circ}2\theta$ ($d = 3.4 \text{ \AA}$), feldspar including both
293 plagioclase and K-feldspar at $27.7^{\circ}2\theta$ ($d = 3.2 \text{ \AA}$), illite including mica at $8.8^{\circ}2\theta$ ($d =$
294 10.1 \AA), chlorite including kaolinite (called “chlorite+kaolinite” hereafter) at $12.4^{\circ}2\theta$ ($d =$
295 7.1 \AA), kaolinite at $24.8^{\circ}2\theta$ ($d = 3.59 \text{ \AA}$) ~~and~~ chlorite at $25.1^{\circ}2\theta$ ($d = 3.54 \text{ \AA}$), and
296 dolomite at $30.9^{\circ}2\theta$ ($d = 2.9 \text{ \AA}$) were determined using MacDiff software (Petschick,
297 2000) based on the peak identification protocols of Biscaye (1965).

298 The mineral ratios used in this study are defined based on XRD peak intensities (PI)
299 as:

300
$$Q/F = \text{quartz/feldspar} = [\text{PI at } 26.6^{\circ}2\theta]/[\text{PI at } 27.7^{\circ}2\theta]$$

301
$$CK/I = (\text{chlorite+kaolinite})/\text{illite} = [\text{PI at } 12.4^{\circ}2\theta]/[\text{PI at } 8.8^{\circ}2\theta]$$

302
$$C/I = \text{chlorite/illite} = [\text{PI at } 25.1^{\circ}2\theta]/[\text{PI at } 8.8^{\circ}2\theta]$$

303
$$K/I = \text{kaolinite/illite} = [\text{PI at } 24.8^{\circ}2\theta]/[\text{PI at } 8.8^{\circ}2\theta]$$

304 The standard error of duplicate analyses in all samples averaged 1.1, 0.08 and 0.05
305 for Q/F, CK/I and C/I ratios, respectively.

306 Clay minerals (less than $2\text{-}\mu\text{m}$ diameter) in core 01A-GC were separated by the
307 settling method based on the Stokes' law (Müller, 1967). To produce an oriented powder
308 X-ray diffractometry (XRD) sample, the collected clay suspensions were
309 vacuum-filtered onto $0.45\text{-}\mu\text{m}$ nitrocellulose filters and dried. Ethylene glycol ($50 \mu\text{l}$)

310 was then soaked onto the oriented clay on the filters. Glycolated sample filters were
311 stored in an oven at 70°C for four hours and then immediately subjected to XRD
312 analyses. Each sample filter was placed directly on a glass slide and X-rayed with a tube
313 voltage of 40 kV and current of 20 mA. Scanning speed was 0.5°/min and the
314 data-sampling step was 0.02° from 2 to 15°. An additional precise scan with a
315 scanning speed of 0.2°/min and sampling step of 0.01° from 24 to 27° was
316 conducted to distinguish chlorite from kaolinite by evaluation of the peaks around
317 25.1° (Elvelhøi and Rønningsland, 1978). The standard errors of duplicate analyses in
318 all samples averaged 0.05 and 0.06 for CK/I and C/I ratios, respectively.

319 The diffraction intensity of chlorite+kaolinite at 7.1 Å was significantly positively
320 correlated with that of chlorite at 3.54 Å ($r = 0.89$), but not with that of kaolinite at 3.59
321 Å ($r = 0.39$) in western Arctic surface sediments (Kobayashi et al., 2016), indicating that
322 the diffraction intensity of chlorite+kaolinite is governed by the amount of chlorite rather
323 than that of kaolinite.

324 Spectral ~~analysis~~analyses of the downcore Q/F and C/I variability ~~was~~were
325 performed using the maximum entropy method provided in the Analyseries software
326 package (Paillard et al., 1996).

327

328 **4. Results**

329 ***4.1. Surface sediments of the Beaufort Sea***

330 Because the dataset of Kobayashi et al. (2016) has only one sample in the eastern
331 Beaufort Sea, we added the data of 16 samples from the eastern Beaufort Sea near the
332 Mackenzie delta and 3 samples from the western Beaufort Sea to fill the gaps in their
333 dataset. More clearly than Kobayashi et al. (2016), the new combined dataset shows that

334 the surface sediments in the eastern Beaufort Sea have the higher Q/F and lower CK/I
335 and C/I ratios than those in the Chukchi Sea (Fig. 2A–C; Supplementary table 1).

336 The Q/F ratio showed a westward decreasing trend from the eastern Beaufort Sea to
337 the East Siberian Sea and its offshore area (Fig. 2D). This supports a notion that
338 quartz-rich but feldspar-poor sediments are derived from the North American margin by
339 the BG circulation, whereas feldspar-rich sediments are delivered to the Chukchi Sea
340 from the Siberian margin by currents along the East Siberian slope (Vogt, 1997; Stein,
341 2008; Darby et al., 2011; Kobayashi et al., 2016).

342 The CK/I and C/I ratios showed a northward decreasing trend in the Chukchi Sea and
343 the Chukchi Borderland (Fig. 2E). ~~This~~ These results are consistent with earlier studies
344 showing that illite is a common clay mineral in Arctic sediments (Kalinenko, 2001;
345 Darby et al., 2011), whereas, chlorite is more abundant in the Bering Sea and the
346 Chukchi shelf areas influenced by the BSI (Naidu and Mowatt, 1983; Kalinenko, 2001;
347 Nwaodua et al., 2014; Kobayashi et al., 2016).

348 These trends support the conclusion of Kobayashi et al. (2016) mentioning that the
349 Q/F ratio can be used as a provenance index for the BG circulation reflecting a
350 westward decrease in its intensity, and the CK/I and C/I ratios can be used as a
351 provenance index for the BSI reflecting a northward decrease in its intensity. The
352 provenance and transportation of these detrital minerals are discussed in detail in Naidu
353 and Mowatt (1983), Kalinenko (2001), Nwaodua et al. (2014) and Kobayashi et al.
354 (2016).

355

356 **4.2. Cores 01A-GC, 05JPC/TC and 06JPC**

357 | Quartz, feldspar, including plagioclase and K-feldspar, illite, chlorite, kaolinite and
358 | dolomite were detected in the study samples. Plagioclase comprises a variety of
359 | anorthite to albite. Microscopic observations of smear slides for the study samples
360 | revealed that quartz and feldspar are the two major minerals in the composition of
361 | detrital grains.

362 | The variation patterns of the Q/F, C/I, CK/I and K/I ratios are different between
363 | fine-grained and glaciomarine units in cores 05JPC/TC and 06JPC (Fig. 3;
364 | Supplementary tables [23–45](#)). The ratios of fine-grained unit are relatively stable
365 | compared with those in glaciomarine units. The higher Q/F ratio in glaciomarine units is
366 | consistent with the finding of previous studies that quartz grains are abundant in the
367 | western Arctic sediments delivered from the Laurentide ice sheet during glacial and
368 | deglacial periods (Bischof et al., 1996; Bischof and Darby, 1997; Phillips and Grantz,
369 | 2001; Kobayashi et al., 2016). Some peaks correspond to dolomite-rich layers (“D” in
370 | Fig. 3). Variation in the K/I ratio was associated with that in the Q/F ratio (Fig. 3),
371 | which is in harmony with an idea that kaolinite was delivered via the Beaufort Gyre
372 | circulation (Kobayashi et al., 2016). The C/I and CK/I ratios are lower in glaciomarine
373 | unit than in fine-grained unit in 06JPC (Fig. 3C), which is consistent with the closure of
374 | Bering Strait in the last glacial (Elias et al., 1992), but this difference is not significant
375 | in 05JPC (Fig. 3B). [High amplitude fluctuations were observed in the C/I and CK/I](#)
376 | [ratios in the fine-grained sediments in 01A-GC and 06JPC \(Fig. 3A and C\). This similar](#)
377 | [fluctuations partly appeared in 05JPC/TC despite its lower sampling resolution \(Fig.](#)
378 | [3B\).](#)

379 | The Q/F ratio in cores 01A-GC, 05JPC/TC and 06JPC shows a gradual long-term
380 | decrease throughout the Holocene (Fig. 4A). In cores 01A-GC and 06JPC studied in

381 more detail, the Q/F ratio also indicates millennial- to century-scale variability (Fig. 4A).
382 Variations of the 5-point running average highlight millennial-scale patterns (Fig. 4A).
383 The variations are generally asynchronous between both cores on this timescale, which
384 strongly depends on their age-depth models.

385 In core 01A-GC, the CK/I and C/I ratios show a general increase after ca. 9.5 ka with
386 the highest values occurring between 6 and 4 ka, and high ratios around 2.5 ka and 1 ka
387 (Fig. 4B). In core 06JPC, the ratios show a general increase after 9.2 ka with higher
388 values occurring between 6 and 3 ka (Fig. 4B). In core 05JPC/TC, slightly higher ratios
389 occur between 6 and 3 ka after a gradual increase from 9.3 ka (Fig. 4B).

390

391 **5. Discussion**

392 ***5.1. Holocene trend in the Beaufort Gyre circulation***

393 The zonal gradient of the Q/F ratio in western Arctic sediments shown in Fig. 2
394 suggests that quartz-rich but feldspar-poor sediments are derived from the North
395 American margin by the BG circulation, whereas feldspar-rich sediments are delivered
396 to the Chukchi Sea from the Siberian margin by currents along the East Siberian slope,
397 and the ratio can be used as an index for the BG circulation reflecting changes in its
398 intensity in sediment-core records (Kobayashi et al., 2016). A consistent upward
399 decrease in the Q/F ratio in three different cores under study (Fig. 4A) suggests that the
400 BG weakened during the Holocene. This pattern is consistent with an orbitally-forced
401 decrease in summer insolation at northern high latitudes from the early Holocene to
402 present. High summer insolation likely melted sea ice in the Canada Basin, in particular
403 in the coastal areas (Fig. 5). The evidence of lower ice concentrations at the Canada
404 Basin margins in the early Holocene was shown in the fossil records of bowhead whale

405 bones from the Beaufort Sea coast (Dyke and Savelle, 2001) and driftwood from
406 northern Greenland (Funder et al., 2011). This condition could decrease the stability of
407 the ice cover at the margins of the Canada Basin, which accelerated the rotation of the
408 BG circulation (Fig. 5), by comparison with observations from recent decades (Shimada
409 et al., 2006). A decrease in summer insolation during the Holocene should have
410 increased the stability of sea-ice cover along the coasts, resulting in the weakening of
411 the BG.

412 Recent observations show that the BG circulation is linked to the AO (Proshutinsky
413 and Johnson, 1997; Rigor et al., 2002). In the negative phase of the AO, the Beaufort
414 High strengthens and intensifies the BG. If the gradual weakening of the BG during the
415 Holocene were attributed to atmospheric circulation only, a concurrent shift in the mean
416 state of the AO from the negative to positive phase would be expected. This view,
417 however, contradicts the existing reconstructions of the AO history showing multiple
418 shifts between the positive and negative phases during the Holocene (e.g., Rimbu et al.,
419 2003; Olsen et al., 2012). We, thus, infer that the decreasing Holocene trend of the BG
420 circulation is attributed not to changes in the AO pattern, but rather to the increasing
421 stability of the sea-ice cover in the Canada Basin.

422 Based on a Holocene sediment record off northeastern Chukchi margin, Darby et al.
423 (2012) suggested strong positive AO-like conditions between 3 and 1.2 ka based on
424 abundant ice-rafted iron oxide grains from the West Siberian shelf. In contrast, a mostly
425 negative AO in the late Holocene can be inferred from mineralogical proxy data
426 indicating a general decline of the BSI after 4 ka (Ortiz et al., 2009), which could be
427 attributed to a stronger Aleutian Low (Danielson et al., 2014) that typically corresponds
428 to the negative AO (Overland et al., 1999). Olsen et al. (2012) also concluded that the

429 AO tended to be mostly negative from 4.2 to 2.0 ka based on a redox proxy record from
430 a Greenland lake. In order to comprehend these patterns, we need to consider not only
431 the atmospheric circulation, but also sea-ice conditions. Based on the Q/F record in this
432 study, summer Arctic sea-ice cover shrank in the early to middle Holocene, so that fast
433 ice containing West Siberian grains could less effectively reach the Canada Basin
434 because sea ice would have melted on the way to the BG (Fig. 5). Later in the Holocene
435 the ice cover expanded, and West Siberian fast ice could survive and be incorporated
436 into the BG (Fig. 5). We infer, therefore, that sediment transportation in the BG is
437 principally governed by the distribution of summer sea ice and the resultant stability of
438 the ice cover in the Canada Basin.

439

440 **5.2. Millennial variability in the BG circulation**

441 In addition to the decreasing long-term trend, the Q/F ratio in 01A-GC and 06JPC
442 clearly displays millennial- to century-scale variability (Fig. 4A). Variation in the Q/F
443 ratio of both 01A-GC and 06JPC indicates a significant periodicity of ~2100 and ~1000
444 years with weak periodicities of ~500 and ~360 years, consistent with prominent
445 periodicities in the variation of total solar irradiance (Fig. 6) (Steinhilber et al., 2009). A
446 comparison with the record of total solar irradiance (Steinhilber et al., 2009) shows a
447 general correspondence, where stronger BG circulation (higher Q/F ratio) corresponds
448 to higher solar irradiance (Fig. 7). A ~200-year phase lag between the solar irradiance
449 and the Q/F ratio in 01A-GC and 06JPC may be attributed to the underestimation of
450 local carbon reservoir effect. This pattern suggests that millennial-scale variability in the
451 BG was principally forced by changes in solar irradiance [as the most likely forcing](#).

452 [Proxy records consistent with solar forcing were reported from a number of](#)

453 paleoclimatic archives, such as Chinese stalagmites (Hu et al., 2008),
454 Jellybean Alaskan Yukon Lake sediments (Anderson et al., 2005); Mt. Logan and ice
455 cores (Fisher et al., 2008), as well as marine sediments in the northwestern Pacific
456 sediments (Sagawa et al., 2014) and the Chukchi Sea sediments (Stein et al., 2017).
457 Because solar forcing is energetically much smaller than changes in the summer
458 insolation caused by orbital forcing, we suppose that solar activity did not directly affect
459 the stability of ice cover in the Canada Basin. Alternatively, we suggest that the solar
460 activity signal was amplified by positive feedback mechanisms, possibly through
461 changes in the stability of sea-ice cover and/or the atmospheric circulation in the
462 northern high latitudes.

463 In addition to cycles consistent with the solar forcing, Darby et al. (2012) reported a
464 1,550 year cycle in the Siberian grain variation in the Chukchi Sea record. This cycle
465 was, however, not detected in our data indicative of the BG variation (Fig. 6). This
466 difference suggests that the occurrence of Siberian grains in the Chukchi Sea sediments
467 primarily reflects the formation and transportation of fast ice in the eastern Arctic Ocean
468 rather than changes in the BG circulation.

469

470 ***5.3. Holocene changes in the Bering Strait Inflow***

471 Northward decreasing trends in the CK/I and C/I ratios in surface sediments in the
472 Chukchi Sea suggests that chlorite-rich sediments are derived from the northern Bering
473 Sea via Bering Strait, and the ratios can be used as an index for the BSI reflecting
474 changes in its intensity in sediment-core records (Kobayashi et al., 2016). Although the
475 variations of the CK/I and C/I ratios are not identical among three study cores (Fig. 4B),
476 there is a common long-term trend showing a gradual increase from 9 to 4.5 ka and a

477 | decrease afterwards (Fig. 4B). Large fluctuations ~~is~~ are significant in 01A-GC from 6 to
478 | 4 ka, and this fluctuation is also seen in 6JPC to some extent (Fig. 4B).

479 | The higher CK/I and C/I ratios in core 01A-GC in the middle Holocene correspond to
480 | higher linear sedimentation rates estimated by interpolation between ¹⁴C dating points,
481 | but this correspondence is not seen in cores 05JPC/TC and 06JPC (Fig. 4C). We assume
482 | that these higher sedimentation rates at 01A-GC indicate intensified BSI, because fine
483 | sediment in the study area is mostly transported by currents from the Bering Sea and
484 | shallow southern Chukchi shelf (Kalinenko, 2001; Darby et al., 2009; Kobayashi et al.,
485 | 2016). The difference of chlorite and sedimentation rate records between 01A-GC and
486 | 05JPC/06JPC may be related to either 1) variable sediment focusing at different water
487 | depths, or 2) redistribution of the BSI water between different branches after passing the
488 | Bering Strait. 1) A sediment-trap study demonstrated that shelf-break eddies in winter
489 | are important to carry fine-grained lithogenic material from the Chukchi Shelf to the
490 | slope areas (Watanabe et al., 2014). This redeposition process may have weakened the
491 | BSI signal in slope sediments of 05JPC/06JPC compared with outer shelf sediments of
492 | 01A-GC. 2) Both the Alaskan Coastal Current (ACC) and the central current can
493 | transport sediment particles to the 05JPC/TC and 06JPC area (red and yellow arrows,
494 | respectively, in Fig. 1; Winsor and Chapman, 2004; Weingartner et al., 2005). In
495 | comparison, the western branch is more likely to carry sediment particles to the site of
496 | 01A-GC (blue arrow in Fig. 1). Redistribution of the BSI water may have caused
497 | different response of BSI signals. Although it is not clear which process made the
498 | difference of BSI signals between 01A-GC and 05JPC/06JPC cores, it is highly possible
499 | that the sedimentation rate and mineral composition of 01A-GC are more sensitive to
500 | changes in BSI intensity than those of two other sites.

501 Diffuse spectral reflectance in core HLY0501-06JPC indicated that chlorite +
502 muscovite content is especially high in the middle Holocene between ca. 4 and 6 ka
503 (Supplementary Fig. S1; Ortiz et al., 2009). However, this pattern was not confirmed by
504 our XRD analysis, where XRD intensities of chlorite and muscovite (detected as illite in
505 this study) as well as the C/I and CK/I ratios did not show an identifiable enrichment
506 between 4 and 6 ka (Supplementary Fig. S1). We need more research to understand the
507 discrepancy of the results.

508

509 ***5.4. Millennial variability in the BSI***

510 Variation in the C/I ratio of 01A-GC indicates a significant periodicity of 1900, 1000,
511 510, 400 and 320 years (Fig. 6A). The 1900, 1000 and 510 years are consistent with
512 prominent periodicities in the variation of total solar irradiance (Fig. 6C) (Steinhilber et
513 al., 2009). On the other hands, variation in the C/I ratio of 06JPC indicates a periodicity
514 of 2200, 830 and 440 years (Fig. 6B). The periodicity is different from that in 01A-GC
515 (Fig. 6A). This suggests that there are different agents of BSI signals in cores 01A-GC
516 and 06JPC. In core 01A-GC, 1000-year filtered variation in the C/I ratio is nearly
517 antiphase with those of the Q/F ratio and total solar irradiance (Steinhilber et al., 2009)
518 between 0 and 5 ka (Fig. 7). This suggests that millennial-scale variability in the
519 western branch of the BSI was forced by changes in solar irradiance after 5 ka. Recent
520 observations demonstrated that the BSI flows northwestward, especially when easterly
521 winds prevent the ACC (Winsor and Chapman, 2004). Because the easterly winds drive
522 the BG circulation, this mechanism cannot explain the increase of BSI intensity when
523 the BG weakened. Alternatively, it is also possible that the solar forcing could

524 independently regulate the western branch of the BSI via unknown atmospheric-oceanic
525 dynamics.

526

527 **5.5. Ocean circulation, sea ice and biological production**

528 The BSI, an important carrier of heat to the Arctic, affects [sea-ice-sea-ice](#) extent in the
529 Chukchi Sea (e.g., Shimada et al., 2006). [Sea-ice](#)[Sea-ice](#) concentrations in the Chukchi
530 Sea during the Holocene were reconstructed by dinoflagellate cysts (de Vernal et al.,
531 2005; 2008; 2013; Farmer et al., 2011) and biomarker IP₂₅ (Polyak et al., 2016; Stein et
532 al., 2017).

533 In central northern Chukchi Sea, IP₂₅ records showed that [sea-ice-sea-ice](#)
534 concentration indicated by PIP₂₅ index in core 01A-GC was lower in 9–7.5 ka and 5.5–4
535 ka (Fig. 8A; Stein et al., 2017), suggesting less [sea-ice-sea-ice](#) conditions in the periods.
536 The low [sea-ice-sea-ice](#) concentration during 9–7.5 ka is consistent with the results of
537 previous studies based on dinoflagellate cyst and IP₂₅ records showing the [sea-ice-sea-ice](#)
538 retreat widely in the Arctic Ocean, which was attributed to higher summer insolation
539 during the early Holocene (Dyke and Savelle, 2001; Vare et al., 2009; de Vernal et al.,
540 2013; Stein et al., 2017). On the other hands, the [sea-ice-sea-ice](#) retreat during 5.5–4 ka
541 cannot be explained by higher summer insolation. This period corresponds to that of
542 higher C/I and CK/I ratios indicative of the stronger BSI at 01A-GC (Fig. 8A). This
543 suggests that the strengthened BSI during this period contributed to [sea-ice-sea-ice](#)
544 retreat in the central Chukchi Sea.

545 In the northeastern Chukchi Sea, dinoflagellate cyst and biomarker IP₂₅ records from
546 several cores in the northeastern Chukchi Sea, including 05JPC, demonstrate that [sea](#)
547 [ice-sea-ice](#) concentration in this area was overall higher in the early Holocene than in the

548 middle and late Holocene (Fig. 8; de Vernal et al., 2005; 2008; 2013; Farmer et al.,
549 | 2011; Polyak et al., 2016). This pattern ~~appears to~~ is in contrast to reconstructions from
550 other Arctic regions that show lower sea-ice concentrations in the early Holocene (de
551 Vernal et al., 2013). This discrepancy suggests that the intensified BG circulation
552 exported more ice from the Beaufort Sea to the northeastern Chukchi Sea margin.
553 Furthermore, the heat transport from the North Pacific to the Arctic Ocean by the BSI
554 was likely weaker in the early Holocene than at later times as indicated by the C/I and
555 CK/I ratios of cores 06JPC and 01A-GC (Fig. 8). We infer that this combination of
556 stronger BG circulation and weaker BSI in the early Holocene resulted in increased
557 sea-ice concentration in the northeastern Chukchi Sea despite high insolation levels (Fig.
558 5). In comparison, intense BSI, a crucial agent of heat transport from the North Pacific
559 | to the Arctic Ocean, along with weaker BG in the middle Holocene likely reduced sea
560 ice cover in the Chukchi Sea. During the late Holocene, characterized by the
561 weakest BG and moderate BSI, sea-ice concentrations were intermediate and strongly
562 variable (Fig. 8; de Vernal et al., 2008, 2013; Polyak et al., 2016).

563 The nutrient supply by the BSI potentially affects marine production in the Chukchi
564 Sea. We tested this possibility to compare our BSI record with marine production
565 records from cores 01A-GC (Park et al., 2016; Stein et al., 2017). Isoprenoid GDGTs
566 | and brassicasterol showed concentration maxima during the periods between 8 and 7.5
567 ka and 6 and 4.5 ka (Fig. 8A). Isoprenoid GDGTs are produced by marine Archaea
568 (Nishihara et al., 1987) that use ammonia, urea and organic matter in the water column
569 (Qin et al., 2014). Brassicasterol is known as a sterol which is abundant in diatoms
570 (Volkman et al., 1986). Their abundance can, thus, be used as proxies to indicate marine
571 production in the water column. The periods with abundant isoprenoid GDGTs and

572 brassicasterol corresponded to the periods of low PIP₂₅ indicative of less sea ice (Fig.
573 8A). This correspondence suggests that the biological productivity increased with the
574 retreat of sea ice in the Chukchi Sea during the middle Holocene. The BSI indices, the
575 C/I and CK/I ratios, showed a maximum between 6 and 4 ka, which corresponded to the
576 periods of high marine production, but the corresponding maximum between 8 and 6.5
577 ka is not significant. Also, correspondence between the BSI indices and biomarker
578 concentrations are not clear after 4 ka. This suggests that marine production was not a
579 simple response to nutrient supply but was affected by other processes such as the
580 increase of irradiance in the water column (Frey et al., 2011; Lee and Whitledge, 2005)
581 and wind-induced mixing that replenishes sea surface nutrients (Carmack et al., 2006).

582

583 ***5.6. Causes of BSI variations***

584 Chukchi Sea sedimentary core records indicate a considerable variability in the BSI
585 intensity, with a common long-term trend of a gradual increase from 9 to 4.5 ka and a
586 decrease afterwards (Fig. 4B). Below we discuss the possible controls on this
587 variability.

588 The timing of the initial postglacial flooding of the ~50-m-deep Bering Strait was
589 estimated as between ca. 12 and 11 ka (Elias et al., 1992; Keigwin et al., 2006;
590 [Jakobsson et al., 2017](#)). Gradual intensification of the BSI inferred from the increase in
591 chlorite content from ca. 9 to 6 ka may have been largely controlled by the widening
592 and deepening of the Bering Strait with rising sea level, although other factors as
593 discussed below yet need to be tested. After the sea level rose to nearly present position
594 by ca. 6 ka, its influence on changes in the BSI volume was negligible.

595 The possible driving forces of the BSI at full interglacial sea level may include
596 several controls. One is related to the sea surface height difference between the Pacific
597 and Atlantic Oceans regulated by the atmospheric moisture transport from the Atlantic
598 to the Pacific Ocean across Central America (Stigebrandt, 1984). Increase in this
599 moisture transport during warm climatic intervals (Leduc et al., 2007; Richter and Xie,
600 2010; Singh et al., 2016) may have intensified the BSI. Salinity proxy data for the last
601 90 ka from the Equatorial East Pacific confirm increased precipitation during warm
602 events, but also show the trans-Central America moisture transport may operate
603 efficiently only during intervals with a northerly position of the Intertropical
604 Convergence Zone due to orographic constraints (Leduc et al., 2007). The existing
605 Holocene salinity records from the North Pacific (e.g., Sarinthein et al., 2004) do not yet
606 provide sufficient material to test the impact of these changes on the BSI.

607 Interplay of the global wind field and the AMOC has been proposed as another
608 potential control on the BSI (De Boer and Nof, 2004; Ortiz et al., 2012). Results of an
609 analytical ocean modeling experiment (Sandal and Nof, 2008) based on the island rule
610 (Godfrey, 1989) suggest that weaker Subantarctic Westerlies in the middle Holocene
611 could decrease the near surface, cross-equatorial flow from the Southern Ocean to the
612 North Atlantic, thus enhancing the BSI and Arctic outflow into the Atlantic. This
613 hypothesis waits to be tested more thoroughly, including robust proxy records of the
614 Subantarctic Westerlies over the Southern Ocean.

615 Finally, BSI can be controlled by the regional wind patterns in the Bering Sea
616 (Danielson et al., 2014), as explained above in Section 2.1. Oceanographic observations
617 of 2000–2011 clearly show a decadal response of the BSI to a change in the sea level
618 pressure in the Aleutian Basin affecting the dynamic sea surface height along the Bering

619 | Strait pressure gradient. In order to conclude, if this relationship holds on longer time
620 | scales, longer-term records are needed from areas affected by the BSI and the Bering
621 | Sea pressure system.

622 | A number of proxy records from the Bering Sea and adjacent regions, both marine
623 | and terrestrial, have been used to characterize paleoclimatic conditions related to
624 | changes in the Bering Sea pressure system (e.g., Barron et al., 2003; Anderson et al.,
625 | 2005; Katsuki et al., 2009; Barron and Anderson, 2011; Osterberg et al., 2014). Various
626 | proxies used in these records consistently show that the Aleutian Low was overall
627 | weaker in the middle Holocene than in the late Holocene, opposite to the BSI strength
628 | inferred from our Chukchi Sea data (Fig. 4B). For example, multi-proxy data from the
629 | interior Alaska and adjacent territories (Kaufman et al., 2016, and references therein)
630 | indicate overall drier and warmer conditions in the middle Holocene, consistent with
631 | weaker Aleutian Low and stronger BSI. Diatom records from southern Bering Sea
632 | indicate more abundant sea ice in the middle Holocene, also suggestive of a weaker
633 | Aleutian Low (Katsuki et al., 2009). Alkenone and diatom records from the California
634 | margin show that the sea surface temperature was lower in the middle Holocene,
635 | suggesting stronger northerly winds indicative of weaker Aleutian Low (Barron et al.,
636 | 2003). Intensification of the Aleutian Low in the late Holocene, which follows from
637 | these results, would have decreased sea level pressure in the Aleutian Basin, and thus
638 | the strength of the BSI, consistent with overall lower BSI after ca. 4 ka inferred from
639 | the Chukchi Sea sediment-core data (Fig. 4). [A-eC](#)onsiderable climate variability of the
640 | Bering Sea region captured in the upper Holocene records, some of which have very
641 | high temporal resolution, is also closely linked to the pressure system changes
642 | (Anderson et al., 2005; Porter, 2013; Osterberg et al., 2014; Steinman et al., 2014). In

643 particular, weakening of the Aleutian Low is reflected in Alaskan ice (Porter, 2013;
644 Osterberg et al., 2014) and lake cores (Anderson et al., 2005; Steinman et al., 2014) at
645 intervals centered around ca. 2 and 1–0.5 ka BP, which may correspond to BSI increases
646 in the Chukchi core 01A-GC at ca. 2.5 and 1 ka BP (Fig. 4), considering the
647 uncertainties of the sparse age constraints in the upper Holocene and/or underestimation
648 of reservoir ages. Overall, the Aleutian Low control on the BSI on century to millennial
649 time scales is corroborated by ample proxy data in comparison with the other potential
650 controls, although more evidence is still required for a comprehensive interpretation.

651

652 ***6. Summary and Conclusions***

653 Distribution of ~~bulk and clay~~ minerals in surficial bottom sediments from the
654 Chukchi Sea shows two distinct trends: an East-West gradient in quartz/feldspar ratios
655 along the shelf margin, and a northwards decrease in the ~~smectite~~chlorite contents.
656 These trends are consistent with the propagation of the Beaufort Gyre circulation in the
657 western Arctic Ocean and the Bering Strait inflow to the Chukchi Sea, respectively.
658 Application of these lithological proxies to sedimentary records from the north-central
659 and northeastern parts of the Chukchi Sea allows for an identification of the Holocene
660 paleoceanographic patterns with century to millennial resolution. Results of the
661 identified ~~Our finding of the~~ Holocene changes in the BG circulation and the BSI in
662 northern Chukchi Sea are summarized in Table 1.

663 The ~~sedimentary proxy based reconstruction of the~~inferred BG weakening during the
664 Holocene, likely driven by the orbitally-controlled summer insolation decrease,
665 indicates basin-wide changes in the Arctic current system and suggests that the stability
666 of sea ice is a key factor regulating the Arctic Ocean circulation on the long-term (e.g.,

667 millennial) time scales. This conclusion helps to better understand a dramatic change in
668 the BG circulation during the last decade, probably caused by sea-ice retreat along the
669 margin of the Canada Basin and a more efficient transfer of the wind momentum to the
670 ice and underlying waters (Shimada et al., 2006). These results suggest that the rotation
671 of the BG is likely to be further accelerated by the projected future retreat of summer
672 Arctic sea ice.

673 The identified Millennial to multi-centennial variability in the BG circulation
674 (quartz/feldspar ratio (the BG circulation)) is consistent with Holocene fluctuations in
675 solar irradiance, suggesting that solar activity affected the BG strength on these
676 timescales.

677 Changes in the BSI inferred from the proxy records show a considerable variability
678 between the investigated sediment cores, likely related to interactions of different
679 current branches and depositional processes. Our results on clay mineral ratios
680 quantifying inputs of chlorite from the Bering Sea to sediments at the northern Chukchi
681 margin provide a robust record of the strength of the BSI during the Holocene. Overall,
682 We conclude that BSI variability after the establishment of the full interglacial sea
683 level in the early Holocene, the BSI variability was primarily largely controlled by the
684 Bering Sea pressure system (strength and position of the Aleutian Low). Details of this
685 mechanism, as well as contributions from other potential BSI controls, such as
686 climatically-driven Atlantic-Pacific moisture transfer and the impact of global wind
687 stress, need to be further investigated. A consistent intensification of the BSI identified
688 in the middle Holocene was associated with a decrease in sea-ice extent and an increase
689 in marine production, indicating a major influence of the BSI on sea ice and biological
690 activity in the Chukchi Sea. In addition, multi-century to millennial fluctuations,

691 | presumably controlled by solar activity, are discernible in core 01A-GC that has been
692 | characterized with the highest age resolution.

693

694 **Acknowledgements**

695 We thank all of the captain, crew and scientists of RV *Araon* for their help during the
696 cruise of sampling. We also thank Yu-Hyeon Park, Anne de Vernal, Seth L. Danielson,
697 Julie Brigham-Grette and Kaustubh Thirumalai for valuable discussion, So-Young Kim,
698 Hyo-Sun Ji, Young-Ju Son, Duk-Ki Han and Hyoung-Jun Kim for assistance in coring
699 and subsampling and Keiko Ohnishi for analytical assistance. [Comments by Martin](#)
700 [Jakobsson, Tomas M. Cronin, and an anonymous reviewer improved greatly this](#)
701 [manuscript.](#) The study was supported by a grant-in-aid for Scientific Research (B) the
702 Japan Society for the Promotion of Science, No. 25287136 (to M.Y.) and Basic
703 Research Project (PE16062) of Korean Polar Research Institute and the NRF of Korea
704 Grant funded by the Korean Government (NRF-2015M1A5A1037243) (to S.I.N.).

705

706 **References**

707 Aagaard, K., Weingartner, T.J., Danielson, S. L., Woodgate, R.A., Johnson, G. C., and
708 Whitley, T.E.: Some controls on flow and salinity in Bering Strait, *Geophysical*
709 *Research Letters*, 33, L19602, 2006.

710 Anderson, L, Abbott, M.B., Finney, B.P., and Burns, S.J.: Regional atmospheric
711 circulation change in the North Pacific during the Holocene inferred from lacustrine
712 carbonate oxygen isotopes, Yukon Territory, Canada, *Quaternary Research*, 64, 21–
713 35, 2005.

714 Barletta, F. et al.: High resolution paleomagnetic secular variation and relative
715 paleointensity records from the western Canadian Arctic: implication for Holocene
716 stratigraphy and geomagnetic field behaviour, *Canadian Journal of Earth Sciences*,
717 45, 1265–1281, 2008.

718 Barron, J.A. and Anderson, L.: Enhanced Late Holocene ENSO/PDO expression along
719 the margins of the eastern North Pacific, *Quaternary International*, 235, 3–12, 2011.

720 Barron, J.A., Heusser, L., Herbert, T., and Lyle, M.: High-resolution climatic evolution
721 of coastal northern California during the past 16,000 years, *Paleoceanography*, 18,
722 1020, 2003.

723 Biscaye, P.: Mineralogy and sedimentation of recent deep-sea clay in the Atlantic Ocean
724 and adjacent seas and oceans, *Geological Society of America Bulletin*, 76, 803–832,
725 1965.

726 Bischof, J., Clark, D.L., and Vincent, J.S.: Origin of ice rafted debris: Pleistocene
727 paleoceanography in the western Arctic Ocean, *Paleoceanography*, 11, 743–756,
728 1996.

729 Bischof, J., and Darby, D.A.: Mid- to Late Pleistocene ice drift in the western Arctic
730 Ocean: Evidence for a different circulation in the Past, *Science*, 277, 74–78, 1997.

731 Carmack, E., Barber, D., Christensen, J., Macdonald, R., Rudels, B., and Sakshaug, E.:
732 2006. Climate variability and physical forcing of the food webs and the carbon
733 budget on pan-Arctic shelves, *Progress in Oceanography*, 71, 145–181, 2006.

734 Coachman, L.K., and Aagaard, K.: On the water exchange through Bering Strait,
735 *Limnology and Oceanography*, 11, 44–59, 1966.

736 Danielson, S.L., Weingartner, T.J., Hedstrom, K.S., Aagaard, K., Woodgate, R.,
737 Curchister, E., and Stabeno, P.J.: Coupled wind-forced controls of the

738 Bering-Chukchi shelf circulation and the Bering Strait throughflow: Ekman
739 transport, continental shelf waves, and variations of the Pacific-Arctic sea surface
740 height gradient, *Progress in Oceanography*, 125, 40–61, 2014.

741 Darby, D.A., Ortiz, J.D., Polyak, L., Lund, S., Jakobsson, M., and Woodgate, R.A.: The
742 role of currents and sea ice in both slowly deposited central Arctic and rapidly
743 deposited Chukchi-Alaskan margin sediments, *Global and Planetary Change*, 68,
744 58–72, 2009.

745 Darby, D.A., Myers, W.B., Jakobsson, M., and Rigor, I.: Modern dirty sea ice
746 characteristic and sources: The role of anchor ice, *Journal of Geophysical Research*,
747 116, C09008, 2011.

748 Darby, D.A., Ortiz, J.D., Grosch, C.E., and Lund, S.P.: 1,500-year cycle in the Arctic
749 Oscillation identified in Holocene Arctic sea-ice drift, *Nature Geoscience*, 5, 897–
750 900, 2012.

751 De Boer, A.M. and Nof, D.: The exhaust valve of the North Atlantic, *Journal of Climate*,
752 17, 417–422, 2004.

753 de Vernal, A., Hillaire-Marcel, C., and Darby, D.A.: Variability of sea ice cover in the
754 Chukchi Sea (western Arctic Ocean) during the Holocene, *Paleoceanography*, 20,
755 PA4018, doi:10.1029/2005PA001157, 2005.

756 de Vernal A, Hillaire-Marcel C, Solignac S, et al.: Reconstructing sea ice conditions in
757 the Arctic and sub-Arctic prior to human observations, *Geophysical Monograph*
758 180, American Geophysical Union, Washington, p. 27–45, 2008.

759 de Vernal, A. et al.: Dinocyst-based reconstructions of sea ice cover concentration
760 during the Holocene in the Arctic Ocean, the northern North Atlantic Ocean and its
761 adjacent seas, *Quaternary Science Reviews*, 79, 111–121, 2013.

762 Dyke, A.S. and Savelle, J.M.: Holocene history of the Bering Sea bowhead whale
763 (*Balaena mysticetus*) in Its Beaufort Sea summer grounds off southwestern Victoria
764 Island, western Canadian Arctic, Quaternary Research, 55, 371–379, 2001.

765 Elias, S., Short, S.K., and Phillips, R.L.: Paleoecology of late-glacial peats from the
766 Bering land bridge, Chukchi Sea shelf region, northwestern Alaska, Quaternary
767 Research, 38, 371–378, 1992.

768 Elvelhøi, A. and Rønningsland, T.M.: Semiquantitative calculation of the relative
769 amounts of kaolinite and chlorite by X-ray diffraction, Marine Geology, 27,
770 M19-M23, 1978.

771 Farmer, J.R., Cronin, T.M., de Vernal, A., Dwyer, G.S., Keigwin, L.D., and Thunell,
772 R.C.: Western Arctic Ocean temperature variability during the last 8000 years,
773 Geophysical Research Letters, 38, L24602, 2011.

774 [Fisher, D., Osterberg, E., Dyke, A., Dahl-Jensen, D., Demuth, M., Zdanowicz, C.,
775 Bourgeois, J., Koerner, R.M., Mayewski, P., Wake, C., Kreutz, K., Steig, E., Zheng,
776 J., Yalcin, K., Goto-Azuma, K., Luckman, B., Rupper, S.: The Mt Logan Holocene–
777 late Wisconsinan isotope record: tropical Pacific–Yukon connections. *Holocene*, 18,
778 667–677, 2008.](#)

779 Frey, K.E., Perovich, D.K., and Light, B.: The spatial distribution of solar radiation
780 under a melting Arctic sea ice cover, Geophysical Research Letters, 38, L22501,
781 2011.

782 Funder, S. et al.: A 10,000-year record of Arctic Ocean sea-ice variability–View from
783 the beach, Science, 333, 747–750, 2011.

784 Giles, K.A. et al.: Western Arctic Ocean freshwater storage increased by wind-driven
785 spin-up of the Beaufort Gyre, Nature Geoscience, 5, 194–197, 2012.

786 Godfrey, J.S.: A sverdrup model of the depth-integrated flow for the ocean allowing for
787 island circulations, *Geophysical and Astrophysical Fluid Dynamics*, 45, 89–112,
788 1989.

789 Griffin, G.M. and Goldberg, E.D.: Clay mineral distributions in the Pacific Ocean. In
790 Hill, M.N. (ed) *The sea*, III, p. 728-741, New York, Interscience Pub., 1963.

791 Gudkovitch, Z.M.: On the nature of the Pacific current in Bering Strait and the cause of
792 its seasonal variations, *Deep-Sea Research*, 9, 507–510, 1962.

793 Harada, N.: Review: Potential catastrophic reduction of sea ice in the western Arctic
794 Ocean: its impact on biogeochemical cycles and marine ecosystems, *Global and*
795 *Planetary Change*, 136, 1–17, 2016.

796 [Hu, C., Henderson, G.M., Huang, J., Xie, S., Sun, Y., Johnson, K.R.: Quantification of](#)
797 [Holocene Asian monsoon rainfall from spatially separated cave records. *Earth and*](#)
798 [Planetary Science Letters](#), 266, 221–232, 2008.

799 [Jakobsson, M., Pearce, C., Cronin, T.M., Backman, J., Anderson, L.G., Barrientos, N.,](#)
800 [Björk, G., Coxall, H., de Boer, A., Mayer, L.A., Mörrh, C.-M., Nilsson, J., Rattray,](#)
801 [J.E., Stranne, C., Semiletov, I., and O'Regan, M.: Post-glacial flooding of the](#)
802 [Beringia land bridge dated to 11,000 cal yrs BP based on new geophysical and](#)
803 [sediment records. *Climate of the Past Discussions*, doi:10.5194/cp-2017-11, 2017.](#)

804 Kaufman, D.S. et al.: Holocene climate changes in eastern Beringia (NW North
805 America) – a systematic review of multi-proxy evidence, *Quaternary Science*
806 *Reviews*, 147, 312–339, 2016.

807 Kalinenko, V.V.: Clay minerals in sediments of the Arctic Seas. *Lith. Min. Res.* 36, 362–
808 372. Translated from *Litologiya i Poleznye Iskopaemye* 4, 418–429, 2001.

809 Katsuki, K., Khim, B.-K., Itaki, T., Harada, N., Sakai, H., Ikeda, T., Takahashi, K.,
810 Okazaki, Y., and Asahi, H.: Land–sea linkage of Holocene paleoclimate on the
811 Southern Bering Continental Shelf, *The Holocene*, 19, 747–756, 2009.

812 Keigwin, L.D., Donnelly, J.P., Cook, M.S., Driscoll, N.W., and Brigham-Grette, J.: Rapid
813 sea-level rise and Holocene climate in the Chukchi Sea, *Geology*, 34, 861–864,
814 2006.

815 Kobayashi, D., Yamamoto, M., Irino, T., Nam, S.-I., Park, Y.-H., Harada, N., Nagashima,
816 K., Chikita, K., and Saitoh, S.-I.: Distribution of detrital minerals and sediment
817 color in western Arctic Ocean and northern Bering Sea sediments: Changes in the
818 provenance of western Arctic Ocean sediments since the last glacial period, *Polar
819 Science*, 10, 519–531, 2016.

820 Leduc, G., Vidal, L., Tachikawa, K., Rostek, F., Sonzogni, C., Beaufort, L. and Bard, E.:
821 Moisture transport across Central America as a positive feedback on abrupt climatic
822 changes, *Nature*, 445, 908–911, doi:10.1038/nature05578, 2007.

823 Lee, S.H., and Whitley, T.E.: Primary and new production in the deep Canada Basin
824 during summer 2002, *Polar Biology*, 28, 190–197, 2005.

825 Lisé-Pronovost, A., St-Onge, G., Brachfeld, S., Barletta, F., and Darby, D.:
826 Paleomagnetic constraints on the Holocene stratigraphy of the Arctic Alaskan margin,
827 *Global and Planetary Change*, 68, 85–99, 2009.

828 McKay, J. L. et al.: Holocene fluctuations in Arctic sea-ice cover: dinocyst-based
829 reconstructions for the eastern Chukchi Sea, *Canadian Journal of Earth Sciences*, 45,
830 1377–1397, 2008.

831 McNeely, R., Dyke, A.S., and Southon, J.R.: Canadian marine reservoir ages,
832 preliminary data assessment, Open File Report-Geological Survey of Canada, 5049,
833 no. 3, 2006.

834 Miller, G.H., Alley, R.B., Brigham-Grette, J., Fitzpatrick, J.J., Polyak, L., Serreze, M.C.,
835 White, J.W.C.: Arctic amplification: can the past constrain the future? Quaternary
836 Science Reviews, 29, 1779–1790, 2010.

837 Müller, G.: Methods in Sedimentary Petrology, Schweizerbart Science Publishers, 283p,
838 Stuttgart, 1967.

839 Naidu, A.S., Creager, J.S., and Mowatt, T.C.: Clay mineral dispersal patterns in the
840 North Bering and Chukchi Seas, Marine Geology, 47, 1-15, 1982.

841 Naidu, A.S. and Mowatt, T.C.: Sources and dispersal patterns of clay minerals in surface
842 sediments from the continental shelf areas off Alaska, Geological Society of
843 America Bulletin, 94, 841–854, 1983.

844 Nishino, S., Shimada, K., Itoh, M., and Chiba, S.: Vertical double silicate maxima in the
845 sea-ice reduction region of the western Arctic Ocean: implications for an enhanced
846 biological pump due to sea-ice reduction, Journal of Oceanography, 60, 871–883,
847 2009.

848 Nishihara, M., Morri, H., and Koga, Y.: Structure determination of a quartet of novel
849 tetraether lipids from *Methanobacterium thermoautotrophicum*, Journal of
850 Biochemistry, 101, 1007–1015, 1987.

851 Nwaodua, E., Ortiz, J.D., and Griffith, E.M.: Diffuse spectral reflectance of surficial
852 sediments indicates sedimentary environments on the shelves of the Bering Sea and
853 western Arctic, Marine Geology, 355, 218–233, 2014.

854 Olsen, J., Anderson, N.J., and Knudsen, M.F.: Variability of the North Atlantic
855 Oscillation over the past 5,200 years, *Nature Geoscience*, 5, 808–812, 2012.

856 Ortiz, J.D., Polyak, L., Grebmeier, J.M., Darby, D., Eberl, D.D., Naidu, S., and Nof, D.:
857 Provenance of Holocene sediment on the Chukchi-Alaskan margin based on
858 combined diffuse spectral reflectance and quantitative X-Ray Diffraction analysis,
859 *Global Planetary Change*, 68, 73–84, 2009.

860 Ortiz, J.D., Nof, D., Polyak, L., St-Onge, G., Lisé-Pronovost, A., Naidu, S., Darby, D.,
861 and Brachfeld, S.: The late Quaternary flow through the Bering Strait has been
862 forced by the Southern Ocean winds, *Journal of Physical Oceanography*, 42, 2014–
863 2029, 2012.

864 Osterberg, E.C., Mayewski, P.A., Fisher, D.A., Kreutz, K.J., Maasch, K.A., Sneed, S.B.,
865 and Kelsey, E.: Mount Logan ice core record of tropical and solar influences on
866 Aleutian Low variability: 500–1998 A.D. *Journal of Geophysical Research*,
867 *Atmosphere*, 119, 11,189–11,204, doi:10.1002/2014JD021847, 2014.

868 Overland, J.O., Adams, J. M., and Bond, N.: Decadal variability of the Aleutian Low
869 and its relation to high-latitude circulation, *Journal of Climate*, 12, 1542–1548,
870 1999.

871 Paillard, D., Labeyrie, L., and Yion, P.: Macintosh program performs time-series
872 analysis, *EOS Trans. AGU* 77, 379, 1996.

873 Park, Y.-H., Yamamoto, M., Polyak, L., and Nam, S.-I.: Glycerol dialkyl glycerol
874 tetraether variations in the northern Chukchi Sea, Arctic Ocean, during the
875 Holocene, *Biogeosciences Discussion*, doi:10.5194/bg-2016-529, 2016.

876 Petschick, R.: MacDiff 4.2.6. [online] available at
877 [http://www.geol-pal.uni-frankfurt.de/Staff/Homepages/Petschick/MacDiff/MacDiff](http://www.geol-pal.uni-frankfurt.de/Staff/Homepages/Petschick/MacDiff/MacDiff%20Latest%20infoE.html)
878 [%20Latest%20infoE.html](http://www.geol-pal.uni-frankfurt.de/Staff/Homepages/Petschick/MacDiff/MacDiff%20Latest%20infoE.html), 2000.

879 Phillips, R.P., and Grantz, A.: Regional variations in provenance and abundance of
880 ice-rafted clasts in Arctic Ocean sediments: implications for the configuration of
881 late Quaternary oceanic and atmospheric circulation in the Arctic, *Marine Geology*
882 172, 91–115, 2001.

883 Pickart, R.S.: Shelfbreak circulation in the Alaskan Beaufort Sea: Mean structure and
884 variability, *Journal of Geophysical Research* 109, C04024, 2004.

885 Pickart, R.S., Pratt, L.J., Torres, D.J., Whitledge, T.E., Proshutinsky, A.Y., Aagaard, K.,
886 Agnewd, T.A., Moore, G.W.K., and Dail, H.J.: Evolution and dynamics of the flow
887 through Herald Canyon in the western Chukchi Sea, *Deep-Sea Research II*, 57, 5–
888 26, 2010.

889 Polyak, L., Bischof, J., Ortiz, J.D., Darby, D.A., Channell, J.E.T., Xuan, C., Kaufman,
890 D.S., Løvile, R., Schneider, D., Eberl, D.D., Adler, R.E., and Council, E.A.: Late
891 Quaternary stratigraphy and sedimentation patterns in the western Arctic Ocean,
892 *Global and Planetary Change*, 68, 5–17, 2009.

893 Polyak, L., Belt, S., Cabedo-Sanz, P., Yamamoto, M., and Park, Y.-H.: Holocene
894 sea-ice conditions and circulation at the Chukchi-Alaskan margin, Arctic Ocean,
895 inferred from biomarker proxies, *The Holocene*, 26, 1810–1821, 2016.

896 Porter, S.E.: Assessing whether climate variability in the Pacific Basin influences the
897 climate over the North Atlantic and Greenland and modulates sea ice extent, Ph.D.
898 Thesis, Ohio State University, 222 p, 2013.

899 Proshutinsky, A.Y. and Johnson, M.A.: Two circulation regimes of the wind-driven
900 Arctic Ocean, *Journal of Geophysical Research*, 102 (C6), 12493–12514, 1997.

901 Qin, W., Amin, S.A., Martens-Habbena, W., Walker, C.B., Urakawa, H., Devol, A.H.,
902 Ingalls, A.E., Moffett, J.M., Armbrust, E.V., and Stahl, D.A.: Marine
903 ammonia-oxidizing archaeal isolates display obligate mixotrophy and wide ecotypic
904 variation. *Proceedings of the National Academy of Science*, 111, 12504–12509,
905 2014.

906 Reimer, P.J., et al.: Intcal13 and Marine13 radiocarbon age calibration curves 0–50,000
907 years cal BP, *Radiocarbon*, 55, 1869–1887, 2013.

908 Richter, I. and Xie, S.: Moisture transport from the Atlantic to the Pacific basin and its
909 response to North Atlantic cooling and global warming, *Climate Dynamics*, 35,
910 551–566, doi:10.1007/s00382-009-0708-3, 2010.

911 Rigor, I. G. et al.: Response of sea ice to the Arctic Oscillation, *Journal of Climate*, 15,
912 2648–2663, 2002.

913 Rimbu, N., Lohmann, G., Kim, J.-H., Arz, H.W., and Schneider, R.: Arctic/North
914 Atlantic Oscillation signature in Holocene sea surface temperature trends as
915 obtained from alkenone data, *Geophysical Research Letters*, 30, 1280.
916 doi:10.1029/2002GL016570, 2003.

917 Roach, A.T., Aagaard, K., Pease, C.H., Salo, S.A., Weingartner, T., Pavlov, V., and
918 Kulakov, M.: Direct measurements of transport and water properties through
919 Bering Strait, *Journal of Geophysical Research*, 100, 18433–18457, 1995.

920 [Sagawa, T., Kuwae, M., Tsuruoka, K., Nakamura, Y., Ikehara, M., and Murayama, M.:](#)
921 [Solar forcing of centennial-scale East Asian winter monsoon variability in the](#)
922 [mid-to late Holocene. *Earth and Planetary Science Letters*, 395, 124–135, 2014.](#)

923 Sakshaug, E.: Primary and secondary production in the Arctic ocean, In: Stein, R.,
924 Macdonald, R.W. (Eds.), *The Organic Carbon Cycle in the Arctic Ocean*, Springer,
925 Berlin, pp. 57–81, 2004.

926 Sandal, C. and Nof, D.: The Collapse of the Bering Strait Ice Dam and the Abrupt
927 Temperature Rise in the Beginning of the Holocene, *Journal of Physical*
928 *Oceanography*, 38, 1979–1991, 2008.

929 Sarnthein, M., Gebhardt, H., Kiefer, T., Kucera, M. Cook, M., and Erlenkeuserd, H.:
930 Mid Holocene origin of the sea-surface salinity low in the subarctic North Pacific,
931 *Quaternary Science Reviews*, 23, 2089–2099, 2004.

932 Screen, J.A. and Simmonds, I.: The central role of diminishing sea ice in recent Arctic
933 temperature amplification, *Nature*, 464, 1334–1337, 2010.

934 Shimada, K., Carmack, E., Hatakeyama, K., and Takizawa, T.: Varieties of shallow
935 temperature maximum waters in the Western Canadian Basin of the Arctic Ocean,
936 *Geophysical Research Letters*, 28, 3441–3444, 2001.

937 Shimada, K., Kamoshida, T., Itoh, M., Nishino, S., Carmack, E., McLaughlin, F.,
938 Zimmermann, S., and Proshutinsky, A.: Pacific Ocean inflow: Influence on
939 catastrophic reduction of sea ice cover in the Arctic Ocean, *Geophysical Research*
940 *Letters*, 33, L08605, 2006.

941 Shtokman, V.B.: Vliyanie vetra na techeniya v Beringovo Prolive, prichiny ikh
942 bol'shikh skorostei i preobladayueshego severnogo napravleniya, *Trans. Inst.*
943 *Okeanolog.*, Akad. Nauk SSSR, 25, 171– 197, 1957.

944 Singh, H.K.A., Donohoe, A., Bitz, C.M., Nusbaumer, J., and Noone, D.C.: Greater
945 aerial moisture transport distances with warming amplify interbasin salinity

946 contrasts. *Geophysical Research Letters* 43, 8677–8684,
947 doi:10.1002/2016GL069796, 2016.

948 Stein R.: *Developments in Marine Geology: Arctic Ocean Sediments: Processes,*
949 *Proxies, and Paleoenvironment*, Elsevier, Amsterdam, 529p, 2008.

950 Stein, R., Fahl, K., Schade, I., Nanerung, A., Wassmuth, S., Niessen, F., and Nam, S.-I.:
951 Holocene variability in sea ice cover, primary production, and Pacific-Water inflow
952 and climate change in the Chukchi and East Siberian Seas (Arctic Ocean), *Journal*
953 *of Quaternary Science*, 32, 362–379, 2017.

954 Steinman, B.A., Abbott, M.B., Mann, M.E., Ortiz, J.D., Feng, S., Pompeani, D.P.,
955 Stansell, N.D., Anderson, L., Finney, B.P., and Bird, B.W.: Ocean-atmosphere
956 forcing of centennial hydroclimate variability in the Pacific Northwest,
957 *Geophysical Research Letters*, 41, doi:10.1002/2014GL059499, 2014.

958 Steinhilber, F., Beer, J., and Fröhlich, C.: Total solar irradiance during the Holocene,
959 *Geophysical Research Letters*, 36, L19704, doi:10.1029/2009GL040142, 2009.

960 Stigebrandt, A.: The North Pacific: A global-scale estuary, *Journal of Physical*
961 *Oceanography*, 14, 464–470, 1984.

962 Vare L.L., Masse G., and Gregory, T.R.: Sea ice variations in the central Canadian
963 Arctic Archipelago during the Holocene, *Quaternary Science Reviews*, 28, 1354–
964 1366, 2009.

965 Viscosi-Shirley, C., Mammone, K., Piasias, N., and Dymond, J.: Clay mineralogy and
966 multi-element chemistry of surface sediments on Siberian-Arctic shelf: implications
967 for sediment provenance and grain size sorting, *Continental Shelf Research*, 23,
968 1175–1200, 2003.

969 Vogt, C.: Regional and temporal variations of mineral assemblages in Arctic Ocean
970 sediments as climatic indicator during glacial/interglacial changes, *Reports on Polar*
971 *Research*, 251, 1–309, 1997.

972 Volkman, J.K.: A review of sterol markers for marine and terrigenous organic matter,
973 *Organic Geochemistry*, 9, 83–99, 1986.

974 Wahsner, M., Müller, C., Stein, R., Ivanov, G., Levitan, M., Shekekhova, E., and
975 Tarasov, G.: Clay-mineral distribution in surface sediments of Eurasian Arctic
976 Ocean and continental margin as indicator for source areas and transport pathways
977 – a synthesis, *Boreas*, 28, 216–233, 1999.

978 Walsh, J.J., and Dieterle, D.A.: CO₂ cycling in the coastal ocean. I. A numerical analysis
979 of the southeastern Bering Sea, with applications to the Chukchi sea and the
980 northern Gulf of Mexico, *Progress in Oceanography*, 34, 335–392, 1994.

981 Watanabe, E., Onodera, J., Harada, N., Honda, M., Kimoto, K., Kikuchi, T., Nishino, S.,
982 Matsuno, K., Yamaguchi, A., Ishida, A., and Kishi, J.M.: Enhanced role of eddies
983 in the Arctic marine biological pump. *Nature Communications*,
984 <http://dx.doi.org/10.1038/ncomms4950>, 2014.

985 Weingartner, T., Aagaard, K., Woodgate, R., Danielson, S., Sasaki, Y., and Cavalieri, D.:
986 Circulation on the north central Chukchi Sea shelf, *Deep-Sea Research II*, 52,
987 3150–3174, 2005.

988 Winsor, P. and Chapman, D.C.: Pathways of Pacific water across the Chukchi Sea: A
989 numerical model study, *Journal of Geophysical Research*, 109, C03002,
990 | [doi:10.1029/2003JC001962](https://doi.org/10.1029/2003JC001962), 2004.

991 [Woodgate, R.A., Weingartner, T.J., and Lindsay, R.: Observed increases in Bering Strait](#)
992 [fluxes from the Pacific to the Arctic from 2001 to 2011 and their impacts on the](#)
993 [Arctic Ocean water column, Geophysical Research Letters, 39, L24603, 2012.](#)

994 Yamamoto-Kawai, M., Carmack, E., and McLaughlin, F.: Nitrogen balance and Arctic
995 throughflow, Nature, 443, 43, 2006

996 _____

Formatted: Indent: Left: 0 cm,
Hanging: 1.77 ch, First line: -1.77
ch

Table 1. Summary of Holocene variability in the BG and BSI in northern Chukchi Sea

<u>Current system</u>	<u>Holocene trends</u>	<u>Multi-centennial to Millennial cyclicality</u>
<u>Beaufort Gyre (BG) circulation</u>	<u>Gradual weakening in response to decreasing summer insolation</u>	<u>0.36, 0.5, 1, and 2-ky cycles paced by changes in solar activity</u>
<u>Bering Strait inflow (BSI)</u>	<u>Geographically variable. Mid-Holocene strengthening evident at the 01A-GC site, presumably due to weaker Aleutian Low</u>	<u>Geographically variable. ~0.36, 0.5, 1, and 2-kyr cycles paced by changes in solar activity are identifiable in 01A-GC</u>

997

998 **Figure captions**

999

1000 Fig. 1. Index map showing location of cores ARA02B 01A-GC (this study),
1001 HLY0501-05JPC/TC (this study and Farmer et al., 2011), HLY0501-06JPC (this study
1002 and Ortiz et al., 2009), and HLY0205-GGC19 (Farmer et al., 2011), as well as surface
1003 sediment samples (Kobayashi et al., 2016, with additions). BSI = Bering Strait inflow,
1004 BC = Barrow Canyon, HN = Hanna Shoal, and HR = Herald Shoal. BG = Beaufort
1005 Gyre, ACC = Alaskan Coastal Current, SBC = Subsurface Boundary Current, ESCC =
1006 East Siberian Coastal Current, TPD = Transpolar Drift. Red, yellow and blue arrows
1007 indicate BSI branches. AO+ and AO- indicate circulation in the positive and negative
1008 phases of the Arctic Oscillation, respectively.

1009

1010 Fig. 2. Spatial distributions of the diffraction intensity ratios of (A) feldspar to quartz
1011 (Q/F), and of (B) chlorite+kaolinite and (C) chlorite to illite (CK/I and C/I, respectively)
1012 of bulk sediments, and (D) the longitudinal distribution of the Q/F ratio in the western
1013 Arctic (>65°N) and (E) the latitudinal distribution of the CK/I and C/I ratios in the
1014 Bering Sea and the western Arctic (>150°W). The C/I ratio could not be determined in
1015 some coarse-grained sediment samples. Data from Kobayashi et al. (2016) with
1016 additions for the Beaufort Sea (See supplementary Table 1 in more detail). [The](#)
1017 [regression lines in panel E show the geographic trends in mineral proxy distribution for](#)
1018 [the Chukchi Sea. The Bering Sea sediments do not show a systematic trend pattern,](#)
1019 [probably reflecting multiple sources of chlorite, such as the Yukon River, Aleutian](#)
1020 [Island, etc. The enlarged maps of the Mackenzie River delta and Yukon River](#)
1021 [estuaries are shown in supplementary Figs. 1 and 2.](#)

1022

1023 Fig. 3. Depth profile in (A) quartz/feldspar (Q/F) ratio, (chlorite + kaolinite)/illite
1024 (CK/I), chlorite/illite (C/I) and kaolinite/illite (K/I) ratios with 1σ -intervals (analytical
1025 error) and the diffraction intensity of dolomite (D) and dolomite intensity in cores (A)
1026 ARA02B 01A-GC, (B) HLY0501-05JPC/TC and (C) HLY0501-06JPC (Supplementary
1027 Tables 2–4). Letter markings “D” in the lower part of 5JPC and 6JPC indicates a
1028 dolomite enriched layers. Note that the depth scale of 01A-GC is doubled. Crosses
1029 represent radiocarbon dates in 01-GC and 5JPC and paleointensity datums in
1030 06JPC. Open circles in Panel B indicate 05TC samples. Note that the depth scale for
1031 01A-GC is doubled for presentation purposes.

1032

1033 Fig. 4. Holocene ~~C~~ changes in (A) quartz/feldspar (Q/F) ratio and the June insolation at
1034 75°N, (B) (chlorite + kaolinite)/illite (CK/I) and chlorite/illite (C/I) ratios, and (C) linear
1035 sedimentation rates (LSR) between age tie points in cores ARA02B 01A-GC,
1036 HLY0501-05JPC/TC and HLY0501-06JPC ~~during the last ca. 9.3 ka. Note that the age~~
1037 model for 06JPC is very tentative, so that a peak in LSR at ca. 2 ka could be an artifact
1038 of spurious age controls.

1039

1040 Fig. 5. Conceptual map showing the distribution of summer sea ice and the rotation of
1041 the Beaufort Gyre (BG) in the early, middle and late Holocene, inferred from the
1042 quartz/feldspar (Q/F) proxy record. Also shown is the Bering Strait inflow (BSI)
1043 intensity inferred from the (chlorite + kaolinite)/illite (CK/I) and chlorite/illite (C/I)
1044 ratios. Red arrow indicates the drift path of Kara Sea grains (KSG; Darby et al., 2012).

1045

1046 Fig. 6. Max Entropy power spectra of variation in the quartz/feldspar (Q/F) and
1047 chlorite/illite (C/I) ratios in core ARA02B 01A-GC (N=85, m=21) and
1048 HYL0501-06JPC (N=79, m=22) during 1.4–7.9 ka and the total solar irradiance (N=932,
1049 m=140)(Steinilber et al., 2009) during the last 9.3 ka.

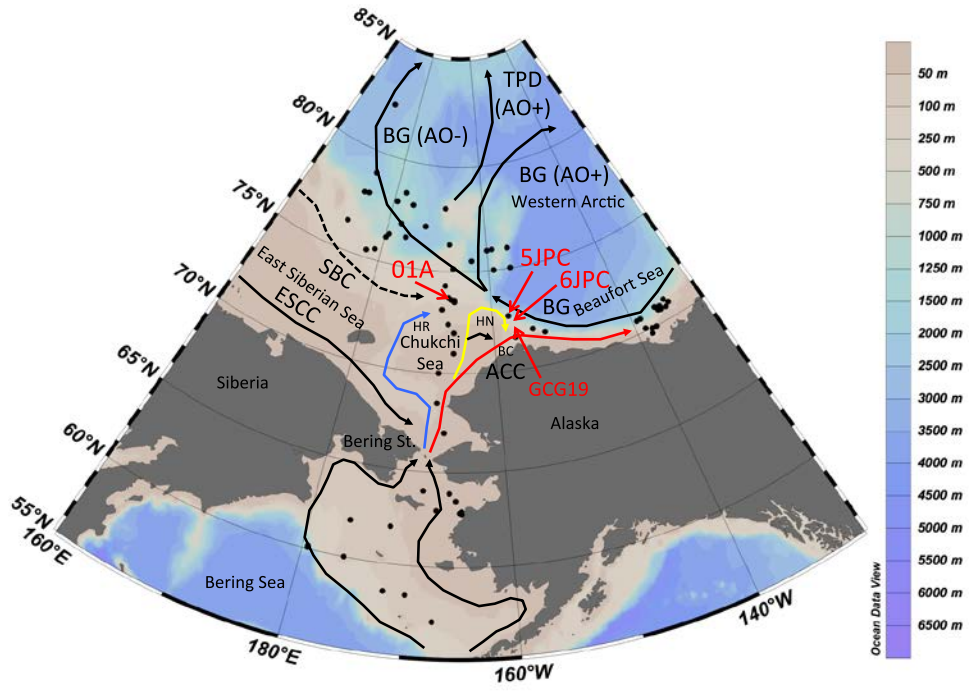
1050

1051 Fig. 7. Detrended variations in the solar irradiance (TSI; Steinilber et al., 2009), the
1052 quartz/feldspar (Q/F) ratio in logarithmic scale in cores ARA02B 01A-GC and
1053 HYL0501-06JPC and the chlorite/illite (C/I) ratio in core ARA02B 01A-GC during the
1054 Holocene, with 400-year moving averages and 1,000-year filtered variations indicated
1055 by dark colored and black lines, respectively. The detrended values were obtained by
1056 cubic polynomial regression.

1057

1058 Fig. 8. Changes in (A) (chlorite + kaolinite)/illite (CK/I) and chlorite/illite (C/I) ratios,
1059 PIP₂₅ (P_DIP₂₅ and P_BIP₂₅ based on IP₂₅ and dinosterol or brassicasterol concentrations)
1060 indices (Stein et al., 2017), and isoprenoid GDGT (Park et al., 2016) and brassicasterol
1061 concentrations (Stein et al., 2017) in core ARA02B 01A-GC, (B) CK/I and C/I ratios in
1062 core HLY0510-5JPC/TC, IP₂₅ concentrations in core HLY0510-5JPC (Polyak et al.,
1063 2016), mean annual duration of sea ice cover concentration (scale from 0 to 10months)
1064 estimated from dinoflagellate cyst assemblages in cores 05JPC and GGC19 (Farmer et
1065 al., 2011; de Vernal et al., 2013).

1066

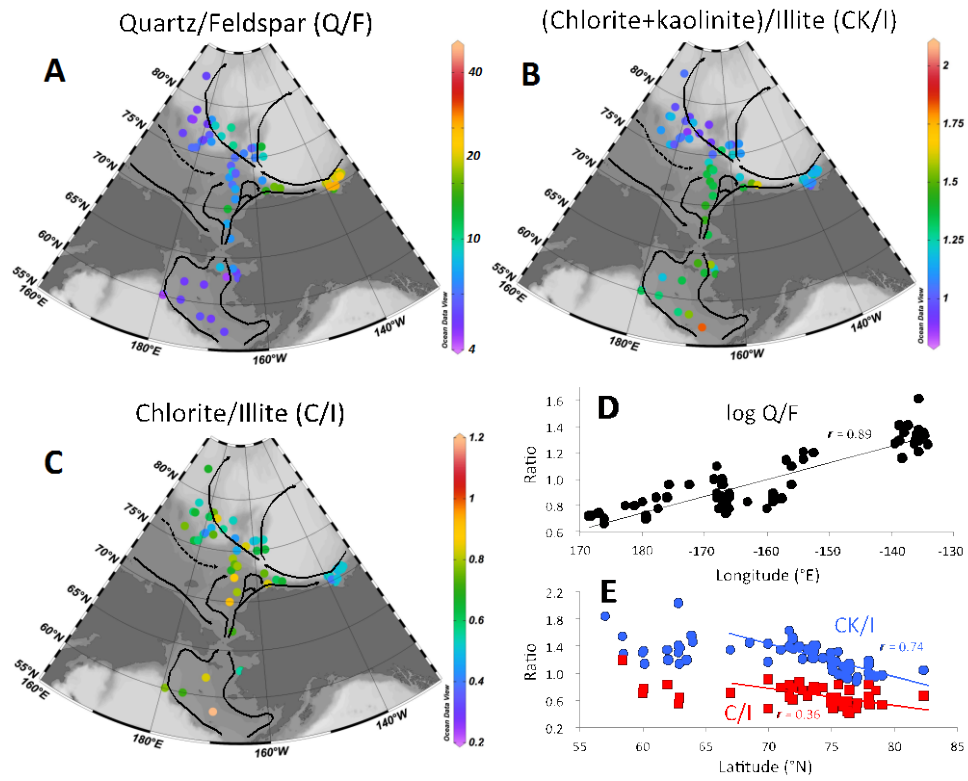


1067

1068

1069 Fig. 1

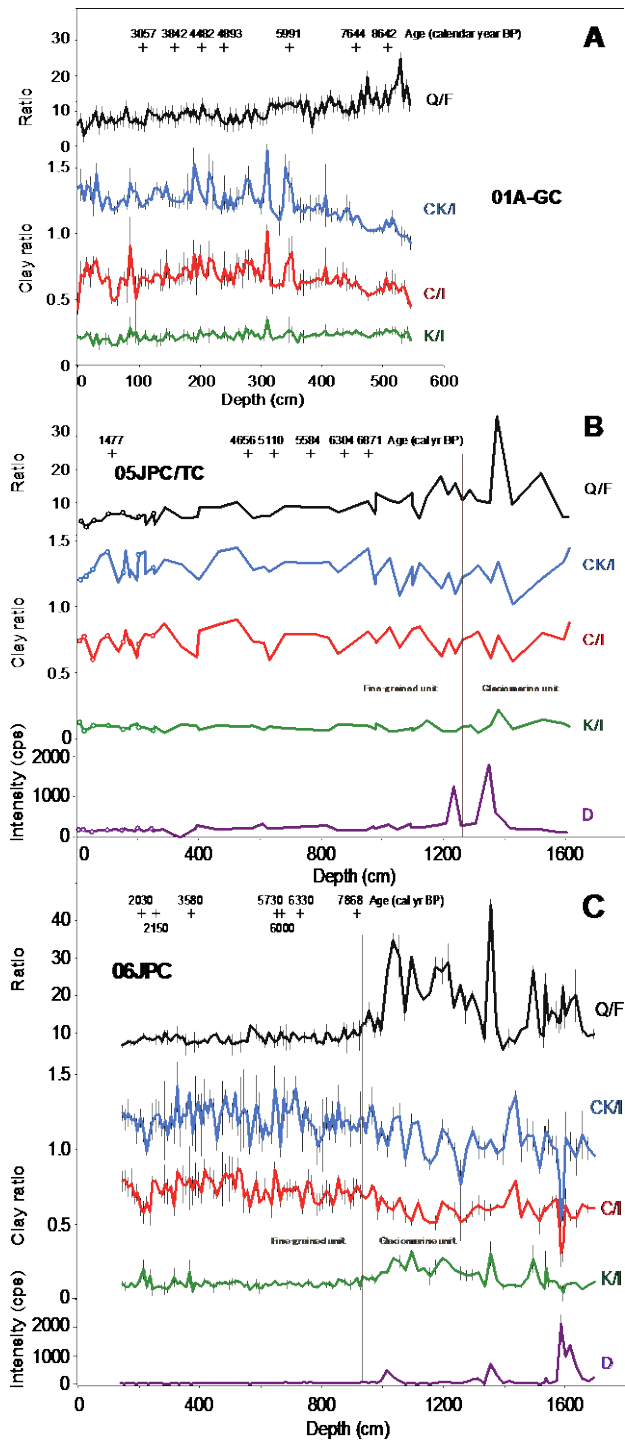
1070



1071

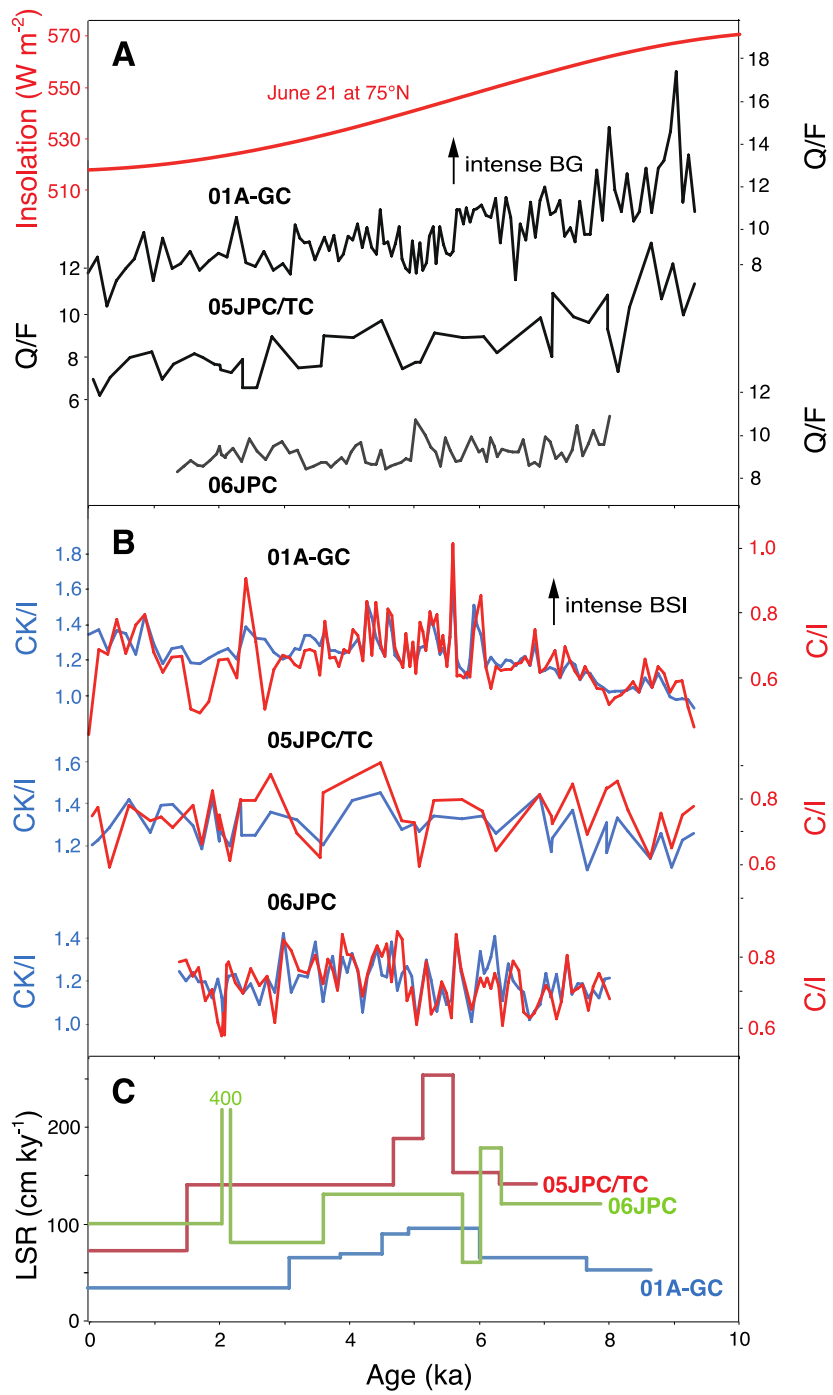
1072 Fig. 2

1073



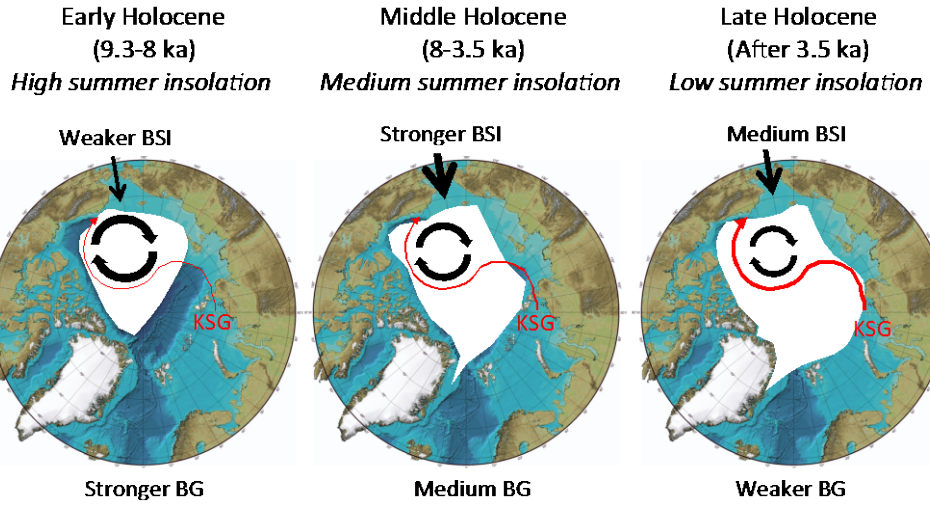
1074

1075 Fig. 3



1076

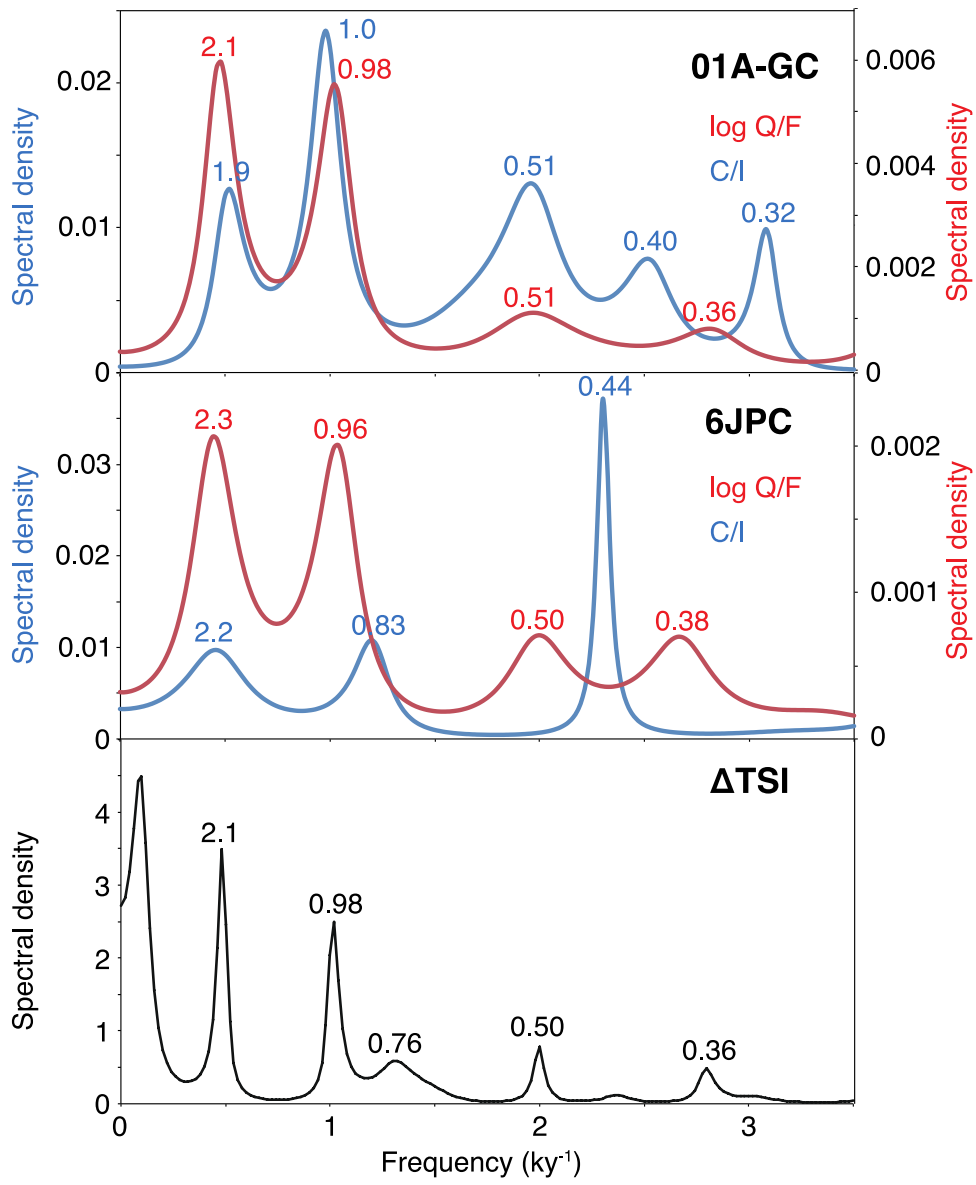
1077 Fig. 4.



1078

1079 Fig. 5

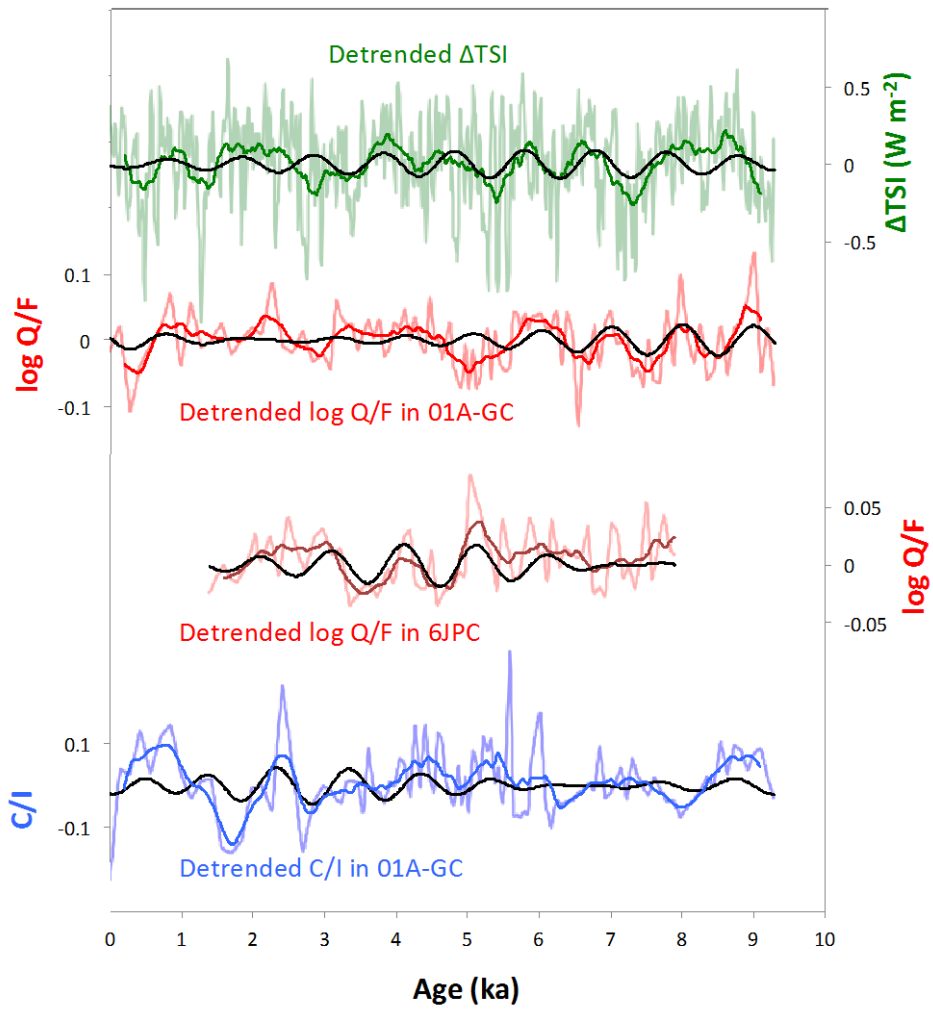
1080



1081

1082 Fig. 6

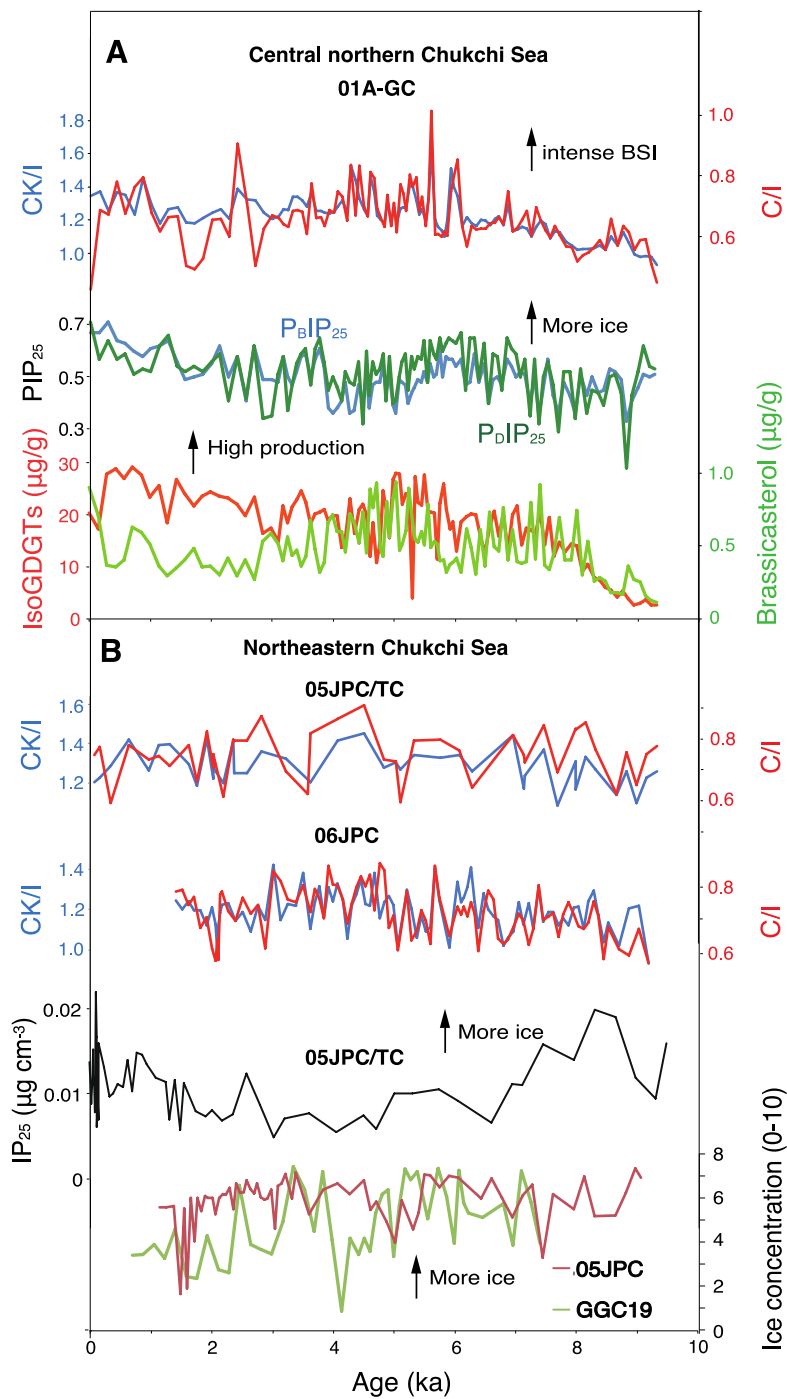
1083



1084

1085 Fig. 7

1086



1087

1088 Fig. 8